

Fig. 1. Organotins Are Agonist Ligands of RXR α and PPAR γ

Organotins are high-affinity ligand agonists of RXR α and PPAR γ . A–D, Activation of GAL4-hRXR α , -hPPAR γ , -hRAR α , or -hPPAR α in transiently transfected Cos7 cells by organotins and receptor-specific ligands. Data represent reporter luciferase activity normalized to β -galactosidase and plotted as the average fold activation \pm SEM ($n = 3$) relative to solvent-only controls from representative experiments. E and F, Competition binding curves of histidine-tagged RXR α or PPAR γ LBDs with TBT. Data shown are from a representative experiment analyzed in GraphPad Prism 4.0 and K_i values deduced (Table 3). Conc, Concentration; DBT, dibutyltin chloride; TROG, troglitazone.

Table 1. TBT Activates RXRs and RXR-Permissive Heterodimers

GAL4-NR LBD	Fold Activation at 60 nM TBT	Permissive RXR Heterodimer
RXR α (<i>Homo sapiens</i>)	60	Yes
RXR α (<i>X. laevis</i>)	25	Yes
RXR γ (<i>X. laevis</i>)	7.0	Yes
NURR1 (<i>H. sapiens</i>)	7.0	Yes
LXR (<i>H. sapiens</i>)	2.1	Yes
PPAR α (<i>Mus musculus</i>)	0.7	Yes
PPAR γ (<i>H. sapiens</i>)	5.3	Yes
PPAR δ (<i>H. sapiens</i>)	1.7	Yes
RAR α (<i>H. sapiens</i>)	0.7	No
TR β (<i>H. sapiens</i>)	0.4	No
VDR (<i>H. sapiens</i>)	0.5	No
SXR (<i>H. sapiens</i>)	1.0	No

Data are fold activation at 60 nM TBT relative to solvent-only controls of transiently transfected Cos7 cells after 24 h ligand treatment. SXR, Steroid and xenobiotic receptor; TR, thyroid hormone receptor.

molar EC₅₀ values. Monobutyltin gave no significant activation whereas dibutyltin was moderately active in the micromolar range (Fig. 1A and Table 2). Tetrabutyltin was 20-fold less potent than TBT, whereas the branched side-chain butyltin tris(2-ethylhexanoate) [BT(2-EHA)₃] was inactive (Table 2). Although activation by dialkyltins is weaker than that of TBT, it is potentially significant due to their widespread use in the manufacture of polyvinyl chloride plastics and greater solubility than TBT.

The effect of the hydrocarbon chain length was very pronounced, suggesting an important structure-activ-

Table 2. Organotin EC₅₀ Values for Nuclear Receptor LBDs

Ligand	GAL4-NR LBD Transactivation (EC ₅₀ Values, nM)		
	hRXR α	hRAR α	hPPAR γ
LGD268	2–5	na	na
AGN195203	0.5–2	na	na
9- <i>cis</i> RA	15	na	na
all- <i>trans</i> RA	na	8	na
Butyltin chloride	na	na	na
Dibutyltin chloride	3000	na	na
TBT	3–8	na	20
Tetrabutyltin	150	ND	ND
Di(triphenyltin)oxide	2–10	na	20
Butyltin tris(2-ethylhexanoate)	na	ND	ND
Troglitazone	na	na	1000
Tributyltin fluoride	3	ND	ND
Tributyltin bromide	4	ND	ND
Tributyltin iodide	4	ND	ND
Triethyltin bromide	2800	ND	ND
Trimethyltin chloride	>10000	ND	ND

na, Not active; ND, not determined. EC₅₀ values were determined from dose-response curves of GAL4-NR LBD construct activation in transiently transfected Cos7 cells after 24-h ligand exposure.

ity relationship. A reduction in hydrophobicity from butyl to ethyl side chains raised the EC₅₀ value by almost 1000-fold into the micromolar range. Trimethyltin was weakly active only above 100 μ M (Table 2). Substitution of the halide component had no significant effect on the EC₅₀ values for TBT, probably due to the lability of the halide atom through exchange in aqueous tissue culture media where chloride ions are prevalent.

TBT Is a Potent Ligand of Both RXR α and PPAR γ

Many, if not most, natural and synthetic nuclear receptor agonists act as ligands that specifically interact with their cognate receptor LBDs. We therefore performed equilibrium competition binding experiments with purified histidine-tagged human RXR α (H₆-RXR α) and PPAR γ (H₆-PPAR γ) LBDs to determine whether the potent and specific activation of these receptors by TBT was due to direct ligand-receptor interaction (Fig. 1, E and F).

The equilibrium binding curves indicate that TBT is a high-affinity, competitive ligand for 9-*cis* RA-bound RXR α . The inhibition equilibrium dissociation constant was calculated by the Chang-Prusoff method [Inhibition constant (K_i) = dissociation constant (K_d)] as 12.5 nM (10–15 nM; 95% confidence interval) (Table 3). By comparison, the value obtained for the synthetic RXR agonist LG100268 was 7.5 nM, which compared favorably with its published value of approximately 3 \pm 1 nM (27). Therefore, the identification of TBT as an RXR ligand expands the molecular definition of known rexinoids (agonists able to activate RXR) to include this structurally unique class of organotin compounds.

Somewhat surprisingly, we also observed potent specific competitive binding by TBT for rosiglitazone bound to human PPAR γ LBD (Fig. 2B). The deduced K_i of 20 nM (17–40 nM; 95% confidence interval) was slightly higher than for RXR α but significantly better than the K_i for the PPAR γ agonist troglitazone, which

Table 3. TBT Binding Constants (K_d) for hRXR α and hPPAR γ LBDs

Ligand	Receptor Competitive Inhibition Binding Constants K _i (nM \pm 95% CI)		
	H ₆ -RXR α	H ₆ -PPAR γ	Published
TBT	12.5 (10–15)	20 (17–40)	
LG100268	7.5 (6–10)	ND	3 \pm 1 ^a
Troglitazone	ND	300 (270–335)	300 \pm 30 ^b

Competition binding curves were determined at constant ³H-specific ligand concentrations [20 nM 9-*cis*-RA, K_d = 1.4 nM (87) or rosiglitazone, K_d = 41 nM (88)] with increasing cold competitor ligands over the range indicated in Fig. 1, E and F. Data were analyzed in GraphPad Prism by nonlinear regression of a competitive one-site binding equation (Chang-Prusoff method) to determine K_i values \pm 95% confidence intervals (n = 3). CI, Confidence interval; ND, not determined.

^a RXR α :LG100268 K_d = 3 \pm 1 nM (27).

^b PPAR γ :troglitazone K_d = 300 \pm 30 nM (28).

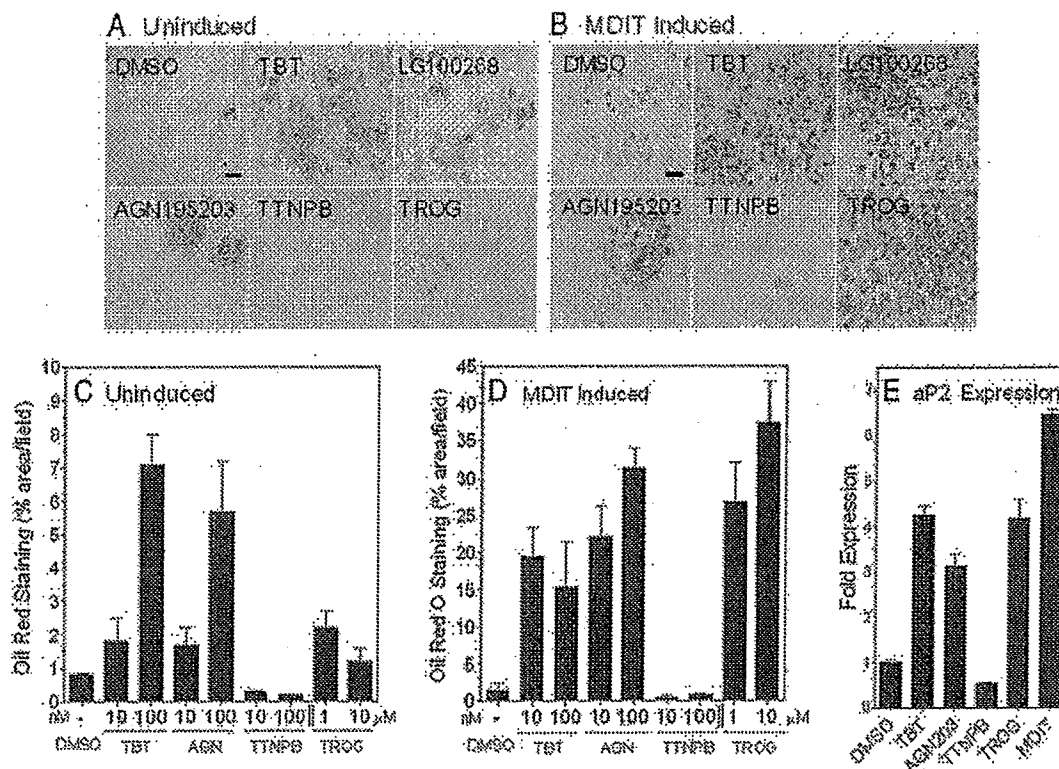


Fig. 2. Tributyltin induces adipogenesis in 3T3-L1 cells

Uninduced (A) and MDIT-induced (B) 3T3-L1 cultures grown for 1 wk in the presence of vehicle (DMSO), or ligands were analyzed for mature adipocyte differentiation by Oil Red O staining. Scale bar represents 100 μ m. C and D, The percentage area stained was determined by automated analysis of random fields ($n = 9$) from high-contrast dissecting scope photographs of monolayers analyzed in ImageJ; 1–100 nM of TBT, AGN195203, and TTNPB or 1–10 μ M troglitazone. E, Quantitative real-time PCR (QRT-PCR) of adipocyte-specific fatty acid binding protein aP2 (aP2/Fabp4) expression levels in postconfluent 3T3-L1 cells treated with the indicated ligands for 24 h. Data were normalized to glyceraldehyde-3-phosphate dehydrogenase controls and plotted as average fold induction \pm SEM ($n = 3$). TROG, Troglitazone.

yielded a K_d of 300 nM, consistent with its published K_d (28). The K_d values for TBT binding to RXR α (12.5 nM) and PPAR γ (20 nM) are also in close agreement with EC₅₀ values obtained from transient transfection assays using GAL4-RXR α and GAL4-PPAR γ constructs (Table 2).

Taken together, these data show that organotin such as TBT, although structurally distinct from previously described natural or synthetic ligands, can interact with RXR α and PPAR γ , via direct ligand binding to induce productive receptor-coactivator interactions and promote transcription in a concentration-dependent manner. Organotin are therefore potent nanomolar receptor activators on par with synthetic RXR and PPAR γ ligands such as LG100268, AGN195203, and thiazolidinediones.

TBT Promotes Adipogenesis in the Murine 3T3-L1 Cell (Embryonic Murine Preadipocyte Fibroblast Cell Line) Model

Numerous studies have demonstrated the critical role played by RXR α :PPAR γ signaling in regulation of

mammalian adipogenesis (29–31). In the murine 3T3-L1 preadipocyte cell model, adipogenic signals induce early key transcriptional regulators such as CCAAT/enhancer binding proteins (C/EBPs) β and δ that lead to mitotic clonal expansion of growth-arrested preadipocytes and induction of the late differentiation factors C/EBP α and PPAR γ (32–34). The combination of C/EBP α expression together with PPAR γ signaling efficiently drives terminal adipocyte differentiation and lipid accumulation. We therefore tested whether TBT signaling through RXR:PPAR γ could promote adipogenesis in the murine 3T3-L1 differentiation assay and compared its effect to other RXR-specific or PPAR γ ligands (Fig. 2). Undifferentiated 3T3-L1 cells were cultured for 1 wk in the presence of ligands either with or without a prior 2-d treatment with MDIT (an adipogenic-sensitizing cocktail of 3-isobutyl-1-methylxanthine, dexamethasone, insulin, and T₃) (35). Cells were then scored for lipid accumulation using Oil Red O staining to determine the degree of terminal adipocyte differentiation. TBT was as effective as LG100268 or AGN195203 in promoting dif-

ferentiation in the absence of MDIT treatment, increasing the number of differentiated adipocytes about 7-fold over solvent-only controls (Fig. 2, A and C). The PPAR γ agonist troglitazone was a weak inducer in the absence of MDIT. Prior treatment with MDIT increased the response to TBT, LG100268, and AGN195203 a further 3- to 5-fold (Fig. 2, B and D). MDIT treatment also boosted the response to troglitazone to equivalent levels as expected from published studies showing that combination treatment with PPAR γ ligands promotes efficient adipocyte differentiation (36–38). In contrast, the RAR agonist TTNPB inhibited the differentiation of 3T3-L1 cells, consistent with previously published data that showed RAR signaling blocks adipogenesis during the early stages of differentiation *in vitro* and can modulate adiposity and whole body weight *in vivo* (39–41). The differential response of 3T3-L1 cells to receptor-selective retinoids indicates that TBT favors RXR homodimer or permissive RXR-heterodimer rather than RXR:RAR signaling in this cell model.

Adipocyte differentiation by TBT was accompanied by direct transcriptional effects on RXR:PPAR γ targets such as adipocyte-specific fatty acid-binding protein (aP2) mRNA. The aP2 promoter contains response elements sensitive to C/EBP factors and RXR α :PPAR γ signaling (42). Quantitative real-time PCR analysis showed aP2 levels were elevated by TBT treatment approximately 5-fold at 24 h (Fig. 2E) and 45-fold at 72 h (data not shown). LG100268, troglitazone, and MDIT treatment also increased aP2 expression at these time points whereas the RAR agonist TTNPB was inhibitory, consistent with the observed cellular responses.

TBT Induces Adipogenic Regulators and Markers of RXR α :PPAR γ Signaling *in Vivo*

The ability of organotins to regulate RXR α :PPAR γ target genes and key modulators of adipogenesis and lipid homeostasis *in vivo* has not been previously examined. Therefore, we next asked whether TBT could perturb expression of critical transcriptional mediators of adipogenesis such as RXR α , PPAR γ , C/EBP $\alpha/\beta/\delta$, and sterol regulatory element binding factor 1 (Srebf1) as well as known target genes of RXR α :PPAR γ signaling from liver, epididymal adipose tissue, and testis of 6-wk-old male mice dosed for 24 h with TBT [0.3 mg/kg body weight (b.w.)], AGN195203 (0.3 mg/kg b.w.), troglitazone (3 mg/kg b.w.), or vehicle (corn oil) administered by ip injection. TBT either had no effect or weakly repressed RXR α and PPAR γ transcription in liver (Fig. 3, A and B). A more pronounced decrease was observed for RXR α , PPAR γ , C/EBP α , and C/EBP δ in adipose tissue and testis (Fig. 3, B and C). In contrast, TBT, AGN195203, and troglitazone significantly induced expression of the early adipogenic transcription factor C/EBP β in liver and testis, whereas it was more weakly induced in adipose tissue. Induction was strongest in testis where TBT and troglitazone

increased expression greater than 10-fold and AGN195203 increased expression 60-fold compared with vehicle controls (Fig. 3C). In addition to C/EBP β , the proadipogenic transcription factor Srebf1 was also significantly increased in adipose tissue by all three receptor ligands and weakly induced in liver.

We also observed coordinate changes in several well-characterized direct target genes of RXR:PPAR γ signaling. Fatty acid transport protein (Fatp) acts as a key control point for regulation of cellular fatty acid content. The Fatp promoter contains a functional PPAR response element shown to be sensitive to RXR:PPAR γ signaling in 3T3-L1 adipocytes and white fat (43–46). Fatp mRNA levels were up regulated 2- to 3-fold in liver and epididymal adipose tissue but not testis by TBT, AGN195203, and troglitazone (see Fig. 5, A and B). Similarly, the PPAR γ target phosphoenolpyruvate carboxykinase 1 (PEPCK/Pck1) (47), the rate-limiting step in hepatic gluconeogenesis and adipose glyceroneogenesis, was up-regulated in liver and adipose tissues by TBT or troglitazone treatment.

Signaling through RXR:PPAR γ , RXR:LXR, and ADD1/Srebf1 in hepatocytes has been shown to modulate fatty acid synthesis through transcriptional control of acetyl-coenzyme A carboxylase (Acac), the rate-limiting step in long-chain fatty acid synthesis (48, 49), as well as fatty acid synthase (Fasn) (50–53). Hepatic expression of both Acac and Fasn was unregulated between 1.5–2.5-fold by TBT, AGN195203, and troglitazone. Therefore, the coordinate increased expression of Fatp, Pck1, Acac, and Fasn in liver suggests that TBT stimulates fatty acid uptake and triglyceride synthesis. Similar changes have been reported in the induction of hepatic steatosis by overactive PPAR γ signaling (49, 54).

Taken together, these data show that TBT exposure induces lipogenic RXR:PPAR γ target gene expression, in adipose tissue and liver, and modulates associated early adipocyte differentiation factors such as C/EBP β and Srebf1. We inferred from these data that organotins are potential adipogenic agents *in vivo*.

Developmental Exposure to TBT Disrupts Lipid Homeostasis and Adipogenesis in Vertebrates

Based on its molecular pharmacology, ability to induce 3T3-L1 adipocyte differentiation, and *in vivo* transcriptional responses, we reasoned that TBT would disrupt normal endocrine control over lipid homeostasis and impact adipogenesis, particularly when exposure occurred during sensitive periods of development. We therefore tested this hypothesis in two vertebrate model systems, mouse and *X. laevis*, during embryogenesis.

Pregnant C57BL/6 mice were injected daily from gestational d 12–18 with TBT (0.05 or 0.5 mg/kg body weight ip) dissolved in sesame oil or vehicle alone. Pups were then killed at birth, and histological sections were prepared from liver, testis, mammary gland, and inguinal adipose tissue. Sections were stained

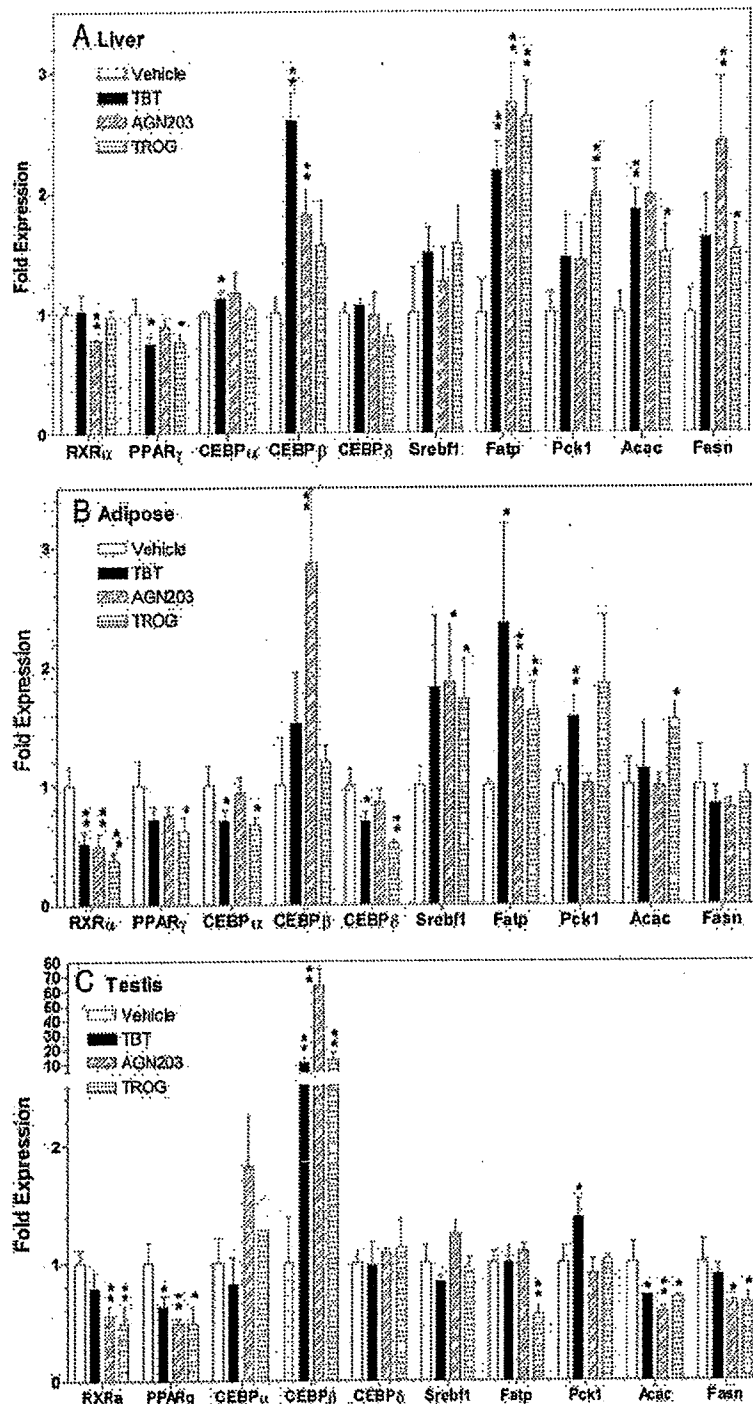


Fig. 3. *In Vivo* Induction of Adipogenic Modulators and RXR:PPAR γ Target Genes

C57BL/6 male mice (three animals per treatment) were dosed with TBT (0.3 mg/kg b.w.), AGN195203 (0.3 mg/kg), troglitazone (3 mg/kg b.w.), or vehicle (corn oil) only by ip injection. Animals were killed after 24 h and dissected and cDNA was prepared from liver, epididymal fat pad, or testis for quantitative real-time PCR analysis. Expression levels were normalized to histone Hist2h4 and shown as the average fold change \pm SEM ($n = 3$) compared with vehicle (corn oil) controls. Control vs. ligand treatments were analyzed by the unpaired Student's *t* test; *, $P < 0.1$; **, $P < 0.05$. TROG, Troglitazone.

with Oil Red O to assess changes in total tissue lipid accumulation. TBT exposure caused a disorganization of hepatic (Fig. 4, A and B) and gonadal (Fig. 4, C and

D) architecture and significantly increased Oil Red O staining in treated animals vs. controls. Liver sections exhibited signs of steatosis consistent with the mis-

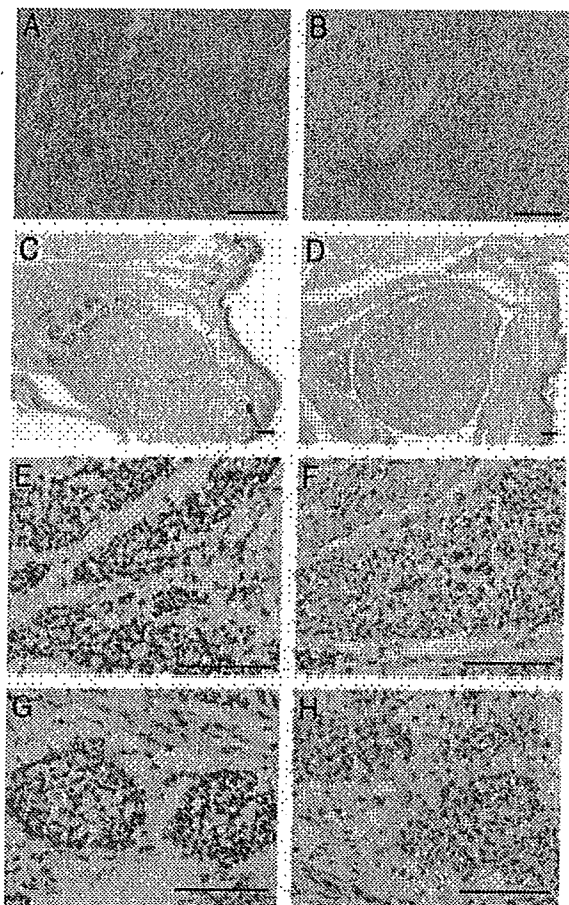


Fig. 4. *In Utero* Exposure to TBT Increases Adiposity in Mouse Liver, Testis, and Adipose Depots

Histological sections (12 μ m) of newborn mouse liver (A and B), testis (C and D), inguinal adipose (E and F) and mammary adipose (G and H) stained with Oil Red O and counterstained with hematoxylin following *in utero* exposure to vehicle only (sesame oil) (A, C, E, and G) or 0.5 mg/kg b.w. TBT (B, D, F, and H) given s.c. daily from E12–18. Scale bar, 100 μ m.

regulation of fatty acid uptake and synthesis observed using molecular markers. In addition, Oil Red O positive staining in mammary and inguinal adipose (Fig. 4, E–H) tissues was dramatically elevated, reflecting either an increase in lipid accumulation or an increase in mature adipocytes.

To determine whether exposure induced long-term changes in growth or adipose tissue, we followed mice from birth to adulthood after *in utero* exposure to TBT as indicated above. At birth, mice were cross-fostered to unexposed dams, and total body weight was recorded until 10 wk of age (Fig. 5A). Growth curves for male and female pups showed a slight trend for lower total body weight consistent with published observations (9) but were not statistically significant at 10 wk [control vs. TBT: male, 26.00 g \pm 0.70 (n = 9) vs. 25.53 g \pm 0.39 (n = 10), P = 0.583; female, 21.22 g \pm 0.41 (n = 10), vs. 20.24 g \pm 0.24 (n = 10), P = 0.0529]. Males were killed at 10 wk and epididymal fat pads were

weighed (Fig. 5B). Adipose mass in TBT-treated males was increased significantly by 20% over controls [control vs. TBT: 0.30 g \pm 0.020 (n = 9) vs. 0.36 g \pm 0.018 (n = 10), P = 0.0374]. These data support the conclusion that TBT can increase body adiposity without overtly increasing total body weight. Similar lipid accumulation and changes in adipose tissue mass have also been observed after TZD or rexinoid treatment (55–57).

We had previously observed that TBT activated *Xenopus* RXRs (Table 1) and reasoned that the strong conservation in vertebrate nuclear receptor signaling pathways should result in consistent responses to organotin and RXR/PPAR γ ligands across diverse vertebrate species. We therefore tested chronic exposure to environmentally relevant low doses of TBT (1–10 nM), the RXR-specific ligands LG100268 and AGN195203 (10–100 nM), troglitazone (0.1–1 μ M), and estradiol (1–10 nM) on developing *X. laevis* tadpoles from stage 48 to metamorphosis. To determine the effectiveness of these doses in *X. laevis* tadpoles, we used aromatase expression as a molecular marker because activity and expression are sensitive to endocrine disruption by organotins and RXR/PPAR γ ligands in mammals (17, 18). *Xenopus* aromatase expression was similarly repressed 2- to 3-fold by 10 nM TBT, AGN195203, LG100268, or 1 μ M troglitazone at stage 56 tadpoles (Fig. 6A) and at all subsequent stages. Despite significant ligand-induced aromatase down-regulation, neither sex ratios nor the time required to reach metamorphosis was altered (data not shown). *Xenopus* liver and kidney also exhibited no gross structural abnormalities at the doses given.

However, consistent with the testis and adipose results from mice presented above, we observed a dose-dependent increase in ectopic adipocyte formation posterior to the fat bodies in and around the gonads of both sexes after TBT or RXR/PPAR γ ligand exposure (Fig. 6B). In contrast, estradiol-treated animals did not show increased adipocyte formation compared with controls. At 10 nM TBT, 10 nM AGN195203, or 1 μ M troglitazone, ectopic adipocytes were observed in approximately 45–60% of animals. At the highest dose of TBT in males, testicular tissue was interspersed with, or replaced by, adipocytes along the anterior-posterior axis (Fig. 6, D, E, and G).

The concordant changes observed in *Xenopus* aromatase expression, gonadal adipocyte formation, and increased murine adiposity after exposure to TBT, RXR and PPAR γ ligands are therefore consistent with a common mechanism of action through RXR:PPAR γ activation, supporting the conclusion that endocrine disruption via nuclear receptor transcriptional regulation is a novel and key feature of organotin toxicity.

DISCUSSION

We have shown above that TBT is a potent inducer of adipogenesis, *in vitro* and *in vivo*, by acting as a novel,

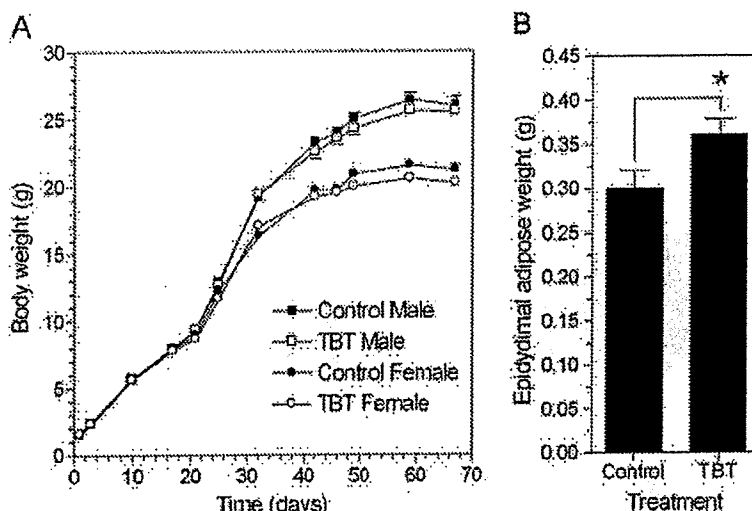


Fig. 5. *In Utero* Exposure to TBT Increases Adipose Mass But Not Body Weight in Adult Mice

A, Growth curves of C57BL/6 male and female pups exposed to control (sesame oil) or TBT *in utero* (E12–18). Data are mean \pm SEM ($n = 10$). B, Epididymal fat pad weights from control or TBT-treated males at 10 wk. *, Epididymal adipose mass from exposed males was approximately 20% greater [control vs. TBT: 0.30 g \pm 0.020 ($n = 9$) vs. 0.36 g \pm 0.018 ($n = 10$); *, $P = 0.0374$]. Data represent mean \pm SEM ($n = 9$ –10).

high-affinity xenobiotic ligand for RXR α and PPAR γ . The ability of organotins to bind and activate these receptors, in particular the RXRs, which exhibit very restricted ligand specificity, is unexpected given the radically different chemical composition and three-dimensional molecular structure of organotins when compared with known natural and synthetic nuclear receptor ligands. Typically, RXR ligands comprise a carboxylic acid functional group and a three-dimensional molecular shape that mimics 9-*cis* RA. Structure-activity profiles indicate distinct structural preferences for organotins but also a relatively broad accommodation for agonist activity that is not easily reconciled with the classical ligand-binding model. Organotins may therefore interact somewhat differently than previously described RXR/PPAR γ ligands with receptor LBDs to induce productive conformational changes required for coactivator recruitment. However, the binding data indicate that TBT is a potent and efficacious ligand for both RXRs and PPAR γ that interacts, at least partially, with the same receptor-binding sites of other high-affinity ligands and promotes the necessary cofactor interactions required for agonist activation. In the study of Kanayama *et al.* (24), TBT was only effective in coactivator recruitment assays with PPAR γ above 10 μ M *in vitro*. However, in accord with our findings, they show that TBT activated PPAR γ significantly at nanomolar concentrations in transfection assays. This may reflect a limitation of preference in the cofactor used *in vitro*. Alternatively, the lower maximal activation observed with TBT on PPAR γ in cells (\sim 30% at 100 nM TBT of troglitazone) is consistent with one of two possibilities: either non-specific cellular toxicity at high levels or activation as a partial agonist.

The ability of TBT to act as a dual ligand for permissive heterodimers such as RXR α :PPAR γ , which can be activated by specific ligands for either receptor, also raises the possibility for additive or synergistic effects that might increase the potency of these compounds *in vivo* at low doses for this specific signaling pathway. Of note is that receptor activation is observed at nanomolar concentrations, whereas other mechanisms of toxicity and endocrine disruption, e.g. direct inhibition of aromatase activity, typically occur in the micromolar range. Furthermore, the activation of other permissive RXR heterodimeric partners, e.g. LXR and NURR1, suggests that organotins may act more widely to disrupt multiple nuclear receptor-mediated hormonal signaling pathways.

The biological consequences of organotin activation of the RXR:PPAR γ signaling pathway are predictable and should follow known aspects of RXR/PPAR γ biology. The RXR:PPAR γ pathway plays a key role in adipocyte differentiation and energy storage, and is central to the control of whole-body metabolism (58). PPAR γ activation increases the expression of genes that promote fatty acid storage and represses genes that induce lipolysis in adipocytes in white adipose tissue (59). PPAR γ such as the thiazolidinediones can modulate insulin sensitivity due to these effects on the adipocyte, reversing insulin resistance in the whole body by sensitizing the muscle and liver tissue to insulin (60). However, a consequence of this increase in whole-body insulin sensitivity is that fat mass is increased through the promotion of triglyceride storage in adipocytes. Evidence is also mounting that depot-specific remodeling and adipocyte numbers increase after thiazolidinedione treatment (55–57). Therefore, PPAR γ agonists comprise a class of phar-

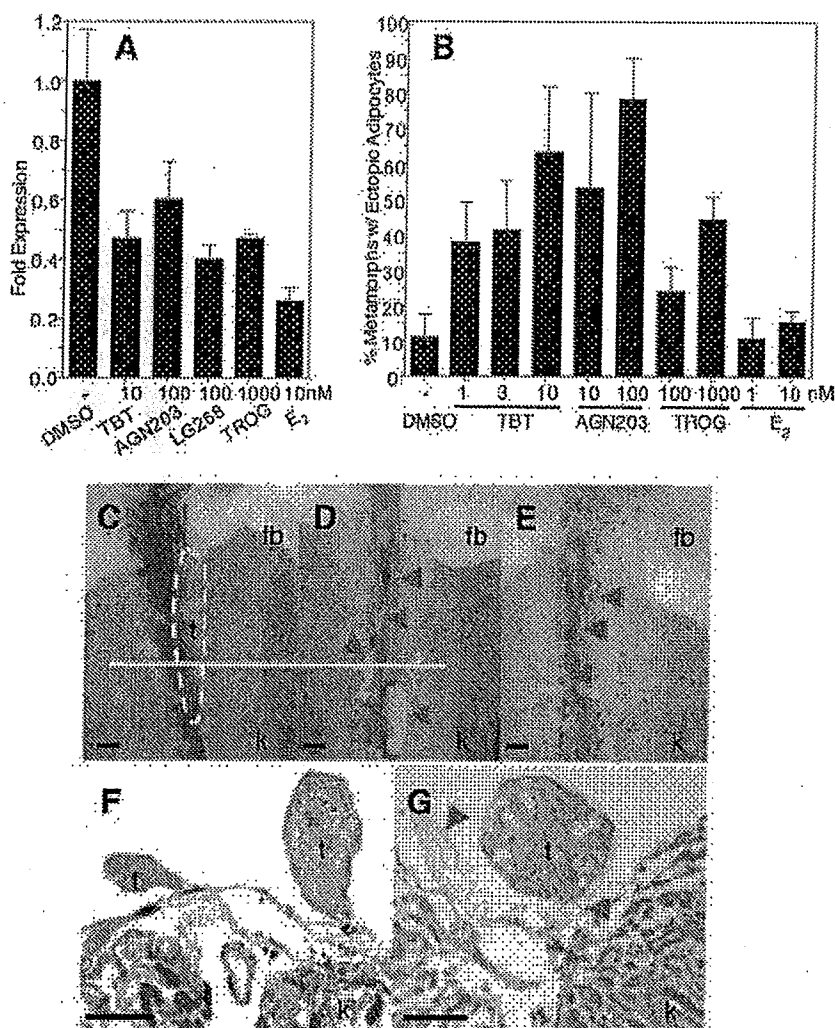


Fig. 6. Endocrine Disruption of RXR:PPAR γ Signaling and Ectopic Induction of Adipocytes in *X. laevis* by TBT

A, Expression levels of *Xenopus* aromatase (XCYP19) were determined in tadpoles (stage 56) by quantitative real-time PCR after 24-h exposure to vehicle only (DMSO) or the indicated ligands. Expression was normalized to *Xenopus* EF1 α and expressed as average fold change in expression \pm SEM ($n = 9$) relative to vehicle controls. B, *X. laevis* tadpoles were dosed weekly under static renewal conditions with indicated ligands from stage 48 (before gonadogenesis) until stage 64 (metamorphic climax). Metamorphs (stage 66) were scored for ectopic adipocyte patches on gonads and urogenital ducts. Data are shown as the percentage of metamorphs exhibiting ectopic adipocyte patches posterior to the fat bodies; mean \pm SD from triplicate tanks. C–E, Dissecting microscope photographs of kidneys (k), testis (t), and fat bodies (fb) from DMSO control, 10 nM TBT, and 1 μ M troglitazone-treated male metamorphs. Multiple ectopic adipocyte patches (red arrows) are present posterior to the fat bodies along the anterior-posterior axis of gonads in TBT (D)- and troglitazone (E)-treated animals but not controls (C). Histological sections of kidneys and gonads from the same control (F) and 10 nM TBT (G)-treated males at the level indicated by the white line in C and D. Gonadal and connective tissue was either completely replaced by, or interspersed with, adipocytes (red arrows) in TBT-treated animals. Sections were developed with Mallory's trichrome stain. Scale bars, 100 μ m.

maceutical therapies for type 2 diabetes that can also promote obesity by increasing fat storage. Likewise, RXR ligands also act as insulin-sensitizing agonists in rodents (61), underscoring the permissive nature of the PPAR γ :RXR heterodimer and the potential effects on diabetes and obesity of both PPAR γ and RXR agonists.

Our data are consistent with recent studies that organotins can mediate some of their endocrine dis-

ruption effects by transcriptional regulation through nuclear receptors, in particular RXR:PPAR γ signaling (17–19, 24). Consequently, TBT exposure can promote adipocyte differentiation in the same manner as other RXR or PPAR γ ligands *in vitro* using the standard murine 3T3-L1 cell model and *in vivo* through increased adiposity after intrauterine organotin exposure in newborn mice. It is currently unknown whether the increased adiposity *in vivo* results from an increase

in adipocyte precursor cell number, enhanced adipocyte differentiation from the same number of precursors, an increase in adipocyte size without an increase in number, or some combination of these.

The prevailing epidemiological data ascribe high-density caloric and/or fatty diets coupled with decreased physical activity as the root causes for the rise in obesity rates in the general population (62). The contribution of genetic components is less clear. Although genetic variation contributes to an individual's propensity to develop obesity, the rapid worldwide increase in obesity suggests that interaction with the modern environment exposes inherent genetic differences. The Barker hypothesis postulates that *in utero* fetal nutritional status is a potential risk factor for metabolic syndrome diseases (63–67). In this view, developmental metabolic programming of a thrifty phenotype limits the range in adaptive responses to the environment, e.g. diet and exercise, in later life (68). Experimental evidence from animal models lends support to this hypothesis (69). Plausible mechanisms include imprinting of obesity-sensitive hormonal pathways or changes in cell type and number, e.g. adipocytes, established during development.

Others, however, argue that the environment plays another role in obesity. Because the increase in obesity rates parallels the rapid growth in the use of industrial chemicals over the past 40 yr, it is plausible and provocative to associate *in utero* or chronic lifetime exposure to chemical triggers present in the modern environment with this epidemic. Hence, an "obesogen" model predicts the existence of xenobiotic chemicals that inappropriately regulate lipid metabolism and adipogenesis to promote obesity. Several recent studies serve as proof-of-principle for such a hypothesis. Environmental estrogens such as bisphenol A and nonylphenol, for instance, can promote adipocyte differentiation or proliferation in murine cell lines (70, 71). Furthermore, epidemiological studies link maternal smoking during pregnancy to an elevated risk of childhood obesity (72–76).

Seen in this context, we propose that organotins such as TBT and its congeners are chemical stressors or obesogens that activate RXR:PPAR γ signaling to promote long-term changes in adipocyte number and/or lipid homeostasis after developmental or chronic lifetime exposure.

MATERIALS AND METHODS

Plasmids and Transfections

pCMX-GAL4 and pCMX-VP16 plasmid fusion constructs to nuclear receptor LBDs and coactivators [GAL4-hRAR α , hRXR α , -xRXR α/γ , -hPPAR γ , -mPPAR α , -human steroid and xenobiotic receptor (SXR), -NURR1, -VDR, -LXR, -hACTR, -hPPAR-binding protein (PBP), -human steroid receptor coactivator-1 (SRC-1), human transcriptional intermediary factor 2 (TIF2)] have been previously described (77–82). Transfections were performed in Cos7 cells (transformed green

monkey kidney fibroblast cell line) essentially as described elsewhere (83) using MH200-x4-TK-Luc as reporter and normalized to pCMX- β -galactosidase controls. Briefly, Cos7 cells were seeded at 5000 cells per well in 96-well tissue culture plates in 10% fetal bovine serum/DMEM and transfected for 8 h with 11 μ g/plate of DNA/calcium phosphate precipitate mix (MH200x4-TK-Luc-CMX- β -galactosidase-nuclear receptor/coactivator effector(s) at a ratio of 5:5:1). Cells were washed free of precipitate with PBS and media were replaced with serum-free insulin, transferrin, lipid, bovine serum albumin supplemented (TLB)/DMEM (84) plus ligands for an additional 24 h before assays for luciferase and β -galactosidase activity. All transfection data points were performed in triplicate, and all experiments were repeated at least three times.

Quantitative Real-Time PCR Analyses

Total cellular RNA from C57BL/6 mouse and *X. laevis* tissues was isolated with Trizol reagent and reversed transcribed with oligo dT and Superscript II (Invitrogen, San Diego, CA) according to the manufacturer's instructions. Triplicate cDNA samples (50 ng/reaction) were analyzed by quantitative real-time PCR on a DNA Engine Opticon thermal cycler [MJ Research (Watertown, MA)/Bio-Rad Laboratories (Hercules, CA)] using SYBR Green chemistry (PerkinElmer Life Sciences, Wellesley, MA). Fold changes in expression levels were calculated after normalization to histone Hist2h4 using the $\Delta\Delta$ cycle threshold method (85). Gene-specific primers were as follows. Hist2h4 forward (F): 5'-CCCGTGGTGTGC-TGAAGGTGTT-3'; reverse (R), 5'-GAATTGAAGCGCGCGC-GTCTA-3'; RXR α F: 5'-CGGCTGCTCAGGGTACTTGTGTTT-3'; R, 5'-CGGCTGCTCAGGGTACTTGTGTTT-3'; PPAR γ F: 5'-TGGGTGAAACTCTGGGAGATTC-3'; R, 5'-AATTTCTTG-TGAAGTGCTCATAGGC-3'; C/EBP α F: 5'-CCAAGAAGTGG-GTGACAAGA-3'; R, 5'-CGGTCATTGTCACTGGTCAACT-3'; C/EBP β F: 5'-GCCCGCCGCTTTAGACC-3'; R, 5'-CG-CTCGTGCTCGCCAATG-3'; C/EBP δ F: 5'-AACCCGCGGC-CTTCTACGAG-3'; R, 5'-ACGGCGGCCATGGAGTCAAT-3'; aP2 F: 5'-GAATTCGATGAAATCACCGCA-3'; R, 5'-CTCTTT-ATTGTGGTGCAGCTTTCCA-3'; FATP F: 5'-AGCCGCTTCTG-GGATGACTGTGT-3'; R, 5'-ACCGAAGCGCTCGTGAA-CTG-3'; ACS F: 5'-CCCAGCCAGTCCCCACCAG-3'; R, 5'-CACACCACTCAGGCTCACACTCGT-3'; FASN F: 5'-TCGG-GTGTGGTGGGTTTGGTGAAT-3'; R, 5'-ACTTGGGGGGCGT-GAGATGTGTTGC-3'; ACAC F: 5'-G GATGGCAGCTCTGGA-GGTGTATG-3'; R, 5'-TGTCCTTAAGCTGGCGGTGTTGTA; Pck1 F: 5'-CTGGCAGCATGGGGTGTGTTGTTAGG-3'; R, 5'-TGCCGAAGTTGTAGCCGAAGAAGG-3'; Srebf1 F: 5'-GCC-CTGCCCCACCTCAAACCT-3'; R, 5'-ACTGGCACGGGCAT-CCTTCTC-3'; *Xenopus* EF1 α F: 5'-GATCCCAGGAAAGC-CAATGTGC 3'; R, 5'-COGGATCCTGCTGCCTTCTTCT-3'; *Xenopus* CYP19 (aromatase) F: 5'-GTCTGGATGAATGGCGG-AAAACA-3'; R, 5'-CTGATGAAGTATGGCCGAATGACC-3'.

Ligand Binding

Histidine-tagged RXR α LBD (H_6 -RXR α LBDs) was expressed and purified from pET15b(+) vector in BL21(DE3) pLysS bacteria cultures after induction with 1 mM isopropyl- β -D-thiogalactopyranoside for 3 h at 37 C (86). Purified H_6 -PPAR γ was purchased from Invitrogen. Proteins were bound to 96-well Nickel Chelate Flashplates (PerkinElmer Life Sciences) at 100 μ g/ml overnight at 4 C and washed five times with 200 μ l/well Flashplate Assay Buffer (20 mM HEPES, pH 7.9; 100 mM KCl, 0.1% cholamidopropyltrimethylammonio-2-hydroxy-1-propanesulfonate, 0.1 mM dithiothreitol). Competition assays typically used 1–5 nM [3 H]-9-*cis*-RA (PerkinElmer Life Sciences) or 10–50 nM [3 H]rosiglitazone (American Radiochemicals, Inc., St. Louis, MO) plus cold competitor ligands in Flashplate Assay Buffer at concentrations indicated in the figures. Plates were incubated at room temperature, pro-

tected from light, and read after 4 h on a Packard Topcount scintillation counter (Packard Instruments, Meriden, CT). Specific bound counts/min were determined by subtraction of counts/min from uncoated wells at each ligand concentration. Data were analyzed with GraphPad Prism 4.0 (GraphPad Software, Inc., San Diego, CA) using a one-site competition binding equation to determine K_d values for competitor ligands; K_d values of 1.4 and 41 nM for 9-*cis*-RA and rosiglitazone for their respective receptors were used in the calculations (87, 88).

3T3-L1 Cell Assays

3T3-L1 (American Type Culture Collection, Manassas, VA) cells were maintained as subconfluent cultures by passage every 3 d from cultures seeded at 5000 cells/cm² in 8% calf serum/DMEM. For differentiation assays, cells were seeded at 15×10^3 cells per well into 24-well tissue culture plates in 8% fetal bovine serum/DMEM, after which cultures were grown for 2 d and then treated with the indicated RXR, RAR, and PPAR ligands either with or without MDIT (100 μ M 3-isobutyl-1-methylxanthine, 100 nM dexamethasone, 0.1 ng/ml insulin, and 2 nM T₃ thyroid hormone) induction cocktail. Media and ligand treatments were renewed every 2 d. After 1 wk, cells were scored for adipocyte differentiation by Oil Red O staining for lipid droplet accumulation. Cultures were washed with PBS, fixed with 10% formaldehyde for 15 min, washed with distilled water, and stained with filtered Oil Red O solution (4 g/liter, 60% isopropanol) for 15 min. Excess stain was removed by washing three times with distilled water. Three random fields from each well were photographed under phase contrast and analyzed in ImageJ. Images were converted into high-contrast black and white images to visualize lipid droplets and scored as the percentage area per field. Data are shown as the mean \pm SEM from three wells per treatment. The method was validated by extraction of Oil Red O from stained cells into 100% isopropanol and quantitated by absorbance at 540 nm on a spectrophotometer.

In Vivo Animal Exposure Experiments

C57BL/6J mice were housed under a 12-h light, 12-h dark cycle. Pregnant mice were dosed by ip injection with TBT [0.05 or 0.5 mg/kg body weight (b.w.)] or vehicle (sesame oil) from embryonic d 12 (E12) every 24 h until the day before delivery. Neonates were killed at the day of delivery and analyzed. The samples were embedded in optimal cutting temperature embedding compound and sectioned (12 mm) using a cryostat. Sections were fixed on slides with 4% paraformaldehyde for 10 min and rinsed in PBS. The slides were then sequentially washed with distilled water and 60% of isopropanol and stained with Oil Red O (4 g/liter, 60% isopropanol). After washing with 60% isopropanol and distilled water, the slides were counterstained with hematoxylin. Sections were evaluated and photographed using a Zeiss microscope (Carl Zeiss, Thornwood, NY).

For long-term growth studies, pups were cross-fostered to unexposed C57BL/6 dams after birth, and litter sizes were kept constant at eight pups per dam (control, two male + two female; TBT treated, two male + two female). Animals were weaned at 3 wk of age and maintained on standard rodent chow. Total body weight was followed until 10 wk of age. Males were then killed, and epididymal fat pads were dissected and weighed.

X. laevis tadpoles were sorted at stage 48 (89) and maintained in 1-liter glass tanks in 20% Holtfreter's buffered salt solution (90) at a density of 10 tadpoles per tank on a diet of ground Tetraamin Fish Flakes and spirulina. Compounds prepared in dimethylsulfoxide (DMSO) as 10³-fold stock solutions were tested on triplicate tanks and dosed by static renewal after weekly water changes. Metamorphs at stage 64

were transferred to individual containers and fed frozen brine shrimp for 2 wk until stage 66. Froglets were euthanized with 250 mg/liter MS222 in 20% Holtfreter's solution and then scored for gonadal abnormalities and interrenal/gonadal adipocyte formation under a dissecting microscope. Kidneys with attached gonads and livers were fixed in 10% formalin-PBS, embedded in paraffin, and sectioned at 15 μ m thickness. Sections were developed with Mallory's trichrome stain.

All animal experiments were approved and performed in accordance with Institutional Animal Care and Use Committee protocols.

Acknowledgments

We thank Drs. I. Blitz, K. Cho, C. Zhou, and T. Osborne for critical reading and comments on the manuscript, Dr. C. Li (Expression Technologies) for the H₆-RXR α LBD construct, and Dr. R. Chandraratna (Allergan Pharmaceuticals, Irvine, CA) for AGN203 and LG268.

Received September 8, 2005. Accepted March 30, 2006.

Address all correspondence and requests for reprints to: Bruce Blumberg, Department of Developmental and Cell Biology, University of California Irvine, 2113 McGaugh Hall, Irvine, California 92697-2300. E-mail: blumberg@uci.edu.

This work was supported by grants from the U.S. Environmental Protection Agency (STAR R830686) and National Institutes of Health (GM-60572) (to B.B.); from the Ministries of Education, Culture, Sports, Science and Technology, Environment and Health Labor and Welfare, Japan (to T.I.); and from the University of California Toxic Substance Research and Training Program (UC-37579) (to F.G.).

F.G., H.W., Z.Z., L.M., K.A., R.C., D.M.G., J.K., T.I. have nothing to declare. B.B. is a named inventor on U.S. patents US 5,861,274, US 6,200,802, and US 6,815,168.

REFERENCES

- Appel KE 2004 Organotin compounds: toxicokinetic aspects. *Drug Metab Rev* 36:763–786
- Golub M, Doherty J 2004 Triphenyltin as a potential human endocrine disruptor. *J Toxicol Environ Health B Crit Rev* 7:281–295
- Blaber S, JM 1970 The occurrence of a penis-like outgrowth behind the right tentacle in spent females of *Nucella lapillus*. *Proc Malacolog Soc London* 39:231–233
- Gibbs P, Bryan G 1986 Reproductive failure in populations of the dog-whelk, *Nucella lapillus*, caused by imposex induced by tributyltin from antifouling paints. *J Mar Biol Assoc UK* 66:767–777
- Matthiessen P, Gibbs P 1998 Critical appraisal of the evidence for tributyltin-mediated endocrine disruption in mollusks. *Environ Toxicol Chem* 17:37–43
- Shimasaki Y, Kitano T, Oshima Y, Inoue S, Imada N, Honjo T 2003 Tributyltin causes masculinization in fish. *Environ Toxicol Chem* 22:141–144
- McAllister BG, Kime DE 2003 Early life exposure to environmental levels of the aromatase inhibitor tributyltin causes masculinisation and irreversible sperm damage in zebrafish (*Danio rerio*). *Aquat Toxicol* 65:309–316
- Omura M, Ogata R, Kubo K, Shimasaki Y, Aou S, Oshima Y, Tanaka A, Hirata M, Makita Y, Inoue N 2001 Two-generation reproductive toxicity study of tributyltin chloride in male rats. *Toxicol Sci* 64:224–232
- Ogata R, Omura M, Shimasaki Y, Kubo K, Oshima Y, Aou S, Inoue N 2001 Two-generation reproductive toxicity

- study of tributyltin chloride in female rats. *J Toxicol Environ Health A* 63:127–144
10. Boyer IJ 1989 Toxicity of dibutyltin, tributyltin and other organotin compounds to humans and to experimental animals. *Toxicology* 55:253–298
 11. Heldrich DD, Steckelbroeck S, Klingmüller D 2001 Inhibition of human cytochrome P450 aromatase activity by butyltins. *Steroids* 66:763–769
 12. Cooke GM 2002 Effect of organotins on human aromatase activity *in vitro*. *Toxicol Lett* 126:121–130
 13. Powers MF, Beavis AD 1991 Triorganotins inhibit the mitochondrial inner membrane anion channel. *J Biol Chem* 266:17250–17256
 14. Gennari A, Viviani B, Galli CL, Marinovich M, Pieters R, Corsini E 2000 Organotins induce apoptosis by disturbance of $[Ca^{2+}]_i$ and mitochondrial activity, causing oxidative stress and activation of caspases in rat thymocytes. *Toxicol Appl Pharmacol* 169:185–190
 15. Philbert MA, Billingsley ML, Reuhl KR 2000 Mechanisms of injury in the central nervous system. *Toxicol Pathol* 28:43–53
 16. Mu YM, Yanase T, Nishi Y, Waseda N, Oda T, Tanaka A, Takayanagi R, Nawata H 2000 Insulin sensitizer, troglitazone, directly inhibits aromatase activity in human ovarian granulosa cells. *Biochem Biophys Res Commun* 271:710–713
 17. Mu YM, Yanase T, Nishi Y, Takayanagi R, Goto K, Nawata H 2001 Combined treatment with specific ligands for PPAR γ :RXR nuclear receptor system markedly inhibits the expression of cytochrome P450arom in human granulosa cancer cells. *Mol Cell Endocrinol* 181:239–248
 18. Saitoh M, Yanase T, Morinaga H, Tanabe M, Mu YM, Nishi Y, Nomura M, Okabe T, Goto K, Takayanagi R, Nawata H 2001 Tributyltin or triphenyltin inhibits aromatase activity in the human granulosa-like tumor cell line KGN. *Biochem Biophys Res Commun* 289:198–204
 19. Nishikawa J, Mamiya S, Kanayama T, Nishikawa T, Shiraishi F, Horiguchi T 2004 Involvement of the retinoid X receptor in the development of imposex caused by organotins in gastropods. *Environ Sci Technol* 38:6271–6276
 20. Baillie-Hamilton PF 2002 Chemical toxins: a hypothesis to explain the global obesity epidemic. *J Altern Complement Med* 8:185–192
 21. Heindel JJ 2003 Endocrine disruptors and the obesity epidemic. *Toxicol Sci* 76:247–249
 22. Jacobs MN, Lewis DF 2002 Steroid hormone receptors and dietary ligands: a selected review. *Proc Nutr Soc* 61:105–122
 23. Watanabe H, Iguchi T, Morohashi K 2002 [Endocrine disruptors and nuclear receptors]. *Nippon Rinsho* 60:397–403
 24. Kanayama T, Kobayashi N, Mamiya S, Nakanishi T, Nishikawa J 2005 Organotin compounds promote adipocyte differentiation as agonists of the peroxisome proliferator-activated receptor γ /retinoid X receptor pathway. *Mol Pharmacol* 67:766–774
 25. Wang Z, Benoit G, Liu J, Prasad S, Aarnisalo P, Liu X, Xu H, Walker NP, Perlmann T 2003 Structure and function of Nurr1 identifies a class of ligand-independent nuclear receptors. *Nature* 423:555–560
 26. Aarnisalo P, Kim CH, Lee JW, Perlmann T 2002 Defining requirements for heterodimerization between the retinoid X receptor and the orphan nuclear receptor Nurr1. *J Biol Chem* 277:35118–35123
 27. Boehm MF, Zhang L, Zhi L, McClurg MR, Berger E, Wagoner M, Mais DE, Suto CM, Davies JA, Heyman RA, Nadzant AM 1995 Design and synthesis of potent retinoid X receptor selective ligands that induce apoptosis in leukemia cells. *J Med Chem* 38:3146–3155
 28. Yu C, Chen L, Luo H, Chen J, Cheng F, Guí C, Zhang R, Shen J, Chen K, Jiang H, Shen X 2004 Binding analyses between human PPAR γ -LBD and ligands. *Eur J Biochem* 271:386–397
 29. Forman BM, Tontonoz P, Chen J, Brun RP, Spiegelman BM, Evans RM 1995 15-Deoxy- δ 12, 14-prostaglandin J2 is a ligand for the adipocyte determination factor PPAR γ . *Cell* 83:803–812
 30. Schoonjans K, Staels B, Auwerx J 1996 The peroxisome proliferator activated receptors (PPARs) and their effects on lipid metabolism and adipocyte differentiation. *Biochim Biophys Acta* 1302:93–109
 31. Kersten S 2002 Peroxisome proliferator activated receptors and obesity. *Eur J Pharmacol* 440:223–234
 32. Lane MD, Tang QQ, Jiang MS 1999 Role of the CCAAT enhancer binding proteins (C/EBPs) in adipocyte differentiation. *Biochem Biophys Res Commun* 266:677–683
 33. Tang QQ, Otto TC, Lane MD 2003 CCAAT/enhancer-binding protein β is required for mitotic clonal expansion during adipogenesis. *Proc Natl Acad Sci USA* 100:850–855
 34. Tang QQ, Lane MD 1999 Activation and centromeric localization of CCAAT/enhancer-binding proteins during the mitotic clonal expansion of adipocyte differentiation. *Genes Dev* 13:2231–2241
 35. Rubin CS, Hirsch A, Fung C, Rosen OM 1978 Development of hormone receptors and hormonal responsiveness *in vitro*. Insulin receptors and insulin sensitivity in the preadipocyte and adipocyte forms of 3T3-L1 cells. *J Biol Chem* 253:7570–7578
 36. Kletzien RF, Clarke SD, Ulrich RG 1992 Enhancement of adipocyte differentiation by an insulin-sensitizing agent. *Mol Pharmacol* 41:393–398
 37. Kletzien RF, Foelimi LA, Harris PK, Wyse BM, Clarke SD 1992 Adipocyte fatty acid-binding protein: regulation of gene expression *in vivo* and *in vitro* by an insulin-sensitizing agent. *Mol Pharmacol* 42:558–562
 38. Tafuri SR 1996 Troglitazone enhances differentiation, basal glucose uptake, and Glut1 protein levels in 3T3-L1 adipocytes. *Endocrinology* 137:4706–4712
 39. Xue JC, Schwarz EJ, Chawla A, Lazar MA 1996 Distinct stages in adipogenesis revealed by retinoid inhibition of differentiation after induction of PPAR γ . *Mol Cell Biol* 16:1567–1575
 40. Kawada T, Kamei Y, Sugimoto E 1996 The possibility of active form of vitamins A and D as suppressors on adipocyte development via ligand-dependent transcriptional regulators. *Int J Obes Relat Metab Disord* 20(Suppl 3):S52–S57
 41. Kawada T, Kamei Y, Fujita A, Hida Y, Takahashi N, Sugimoto E, Fushiki T 2000 Carotenoids and retinoids as suppressors on adipocyte differentiation via nuclear receptors. *Biofactors* 13:103–109
 42. Tontonoz P, Graves RA, Budavari AI, Erdjument-Bromage H, Lui M, Hu E, Tempst P, Spiegelman BM 1994 Adipocyte-specific transcription factor ARF6 is a heterodimeric complex of two nuclear hormone receptors, PPAR γ and RXR α . *Nucleic Acids Res* 22:5628–5634
 43. Martin G, Schoonjans K, Lefebvre AM, Staels B, Auwerx J 1997 Coordinate regulation of the expression of the fatty acid transport protein and acyl-CoA synthetase genes by PPAR α and PPAR γ activators. *J Biol Chem* 272:28210–28217
 44. Motojima K, Passilly P, Peters JM, Gonzalez FJ, Latruffe N 1998 Expression of putative fatty acid transporter genes are regulated by peroxisome proliferator-activated receptor α and γ activators in a tissue- and inducer-specific manner. *J Biol Chem* 273:16710–16714
 45. Frohner BI, Hui TY, Bernlohr DA 1999 Identification of a functional peroxisome proliferator-responsive element in the murine fatty acid transport protein gene. *J Biol Chem* 274:3970–3977
 46. Martin G, Poirier H, Hennuyer N, Crombie D, Fruchart JC, Heyman RA, Besnard P, Auwerx J 2000 Induction of the fatty acid transport protein 1 and acyl-CoA synthase

- genes by dimer-selective retinoids suggests that the peroxisome proliferator-activated receptor-retinoid X receptor heterodimer is their molecular target. *J Biol Chem* 275:12612–12618
47. Tontonoz P, Hu E, Devine J, Beale EG, Spiegelman BM 1995 PPAR γ 2 regulates adipose expression of the phosphoenolpyruvate carboxykinase gene. *Mol Cell Biol* 15:351–357
 48. Magana MM, Lin SS, Dooley KA, Osborne TF 1997 Sterol regulation of acetyl coenzyme A carboxylase promoter requires two interdependent binding sites for sterol regulatory element binding proteins. *J Lipid Res* 38:1630–1638
 49. Schadinger SE, Bucher NL, Schreiber BM, Farmer SR 2005 PPAR γ 2 regulates lipogenesis and lipid accumulation in steatotic hepatocytes. *Am J Physiol Endocrinol Metab* 288:E1195–E1205
 50. Tontonoz P, Kim JB, Graves RA, Spiegelman BM 1993 ADD1: a novel helix-loop-helix transcription factor associated with adipocyte determination and differentiation. *Mol Cell Biol* 13:4753–4759
 51. Kim JB, Spiegelman BM 1996 ADD1/SREBP1 promotes adipocyte differentiation and gene expression linked to fatty acid metabolism. *Genes Dev* 10:1096–1107
 52. Joseph SB, Laffitte BA, Patel PH, Watson MA, Matsuoka KE, Walczak R, Collins JL, Osborne TF, Tontonoz P 2002 Direct and indirect mechanisms for regulation of fatty acid synthase gene expression by liver X receptors. *J Biol Chem* 277:11019–11025
 53. Seo JB, Moon HM, Kim WS, Lee YS, Jeong HW, Yoo EJ, Ham J, Kang H, Park MG, Steffensen KR, Stulnig TM, Gustafsson JA, Park SD, Kim JB 2004 Activated liver X receptors stimulate adipocyte differentiation through induction of peroxisome proliferator-activated receptor γ expression. *Mol Cell Biol* 24:3430–3444
 54. Yu S, Matsusue K, Kashireddy P, Cao WQ, Yeldandi V, Yeldandi AV, Rao MS, Gonzalez FJ, Reddy JK 2003 Adipocyte-specific gene expression and adipogenic stasis in the mouse liver due to peroxisome proliferator-activated receptor γ 1 (PPAR γ 1) overexpression. *J Biol Chem* 278:498–505
 55. Hallakou S, Doare L, Fougelle F, Kergoat M, Guerre-Millo M, Berthault MF, Dugail I, Morin J, Auwerx J, Ferre P 1997 Pioglitazone induces in vivo adipocyte differentiation in the obese Zucker fa/fa rat. *Diabetes* 46:1393–1399
 56. de Souza CJ, Eckhardt M, Gagen K, Dong M, Chen W, Laurent D, Burkley BF 2001 Effects of pioglitazone on adipose tissue remodeling within the setting of obesity and insulin resistance. *Diabetes* 50:1863–1871
 57. Smith SR, De Jonge L, Volaufova J, Li Y, Xie H, Bray GA 2005 Effect of pioglitazone on body composition and energy expenditure: a randomized controlled trial. *Metabolism* 54:24–32
 58. Auwerx J 1999 PPAR γ , the ultimate thrifty gene. *Diabetologia* 42:1033–1049
 59. Ferre P 2004 The biology of peroxisome proliferator-activated receptors: relationship with lipid metabolism and insulin sensitivity. *Diabetes* 53(Suppl 1):S43–S50
 60. Day C 1999 Thiazolidinediones: a new class of antidiabetic drugs. *Diabet Med* 16:179–192
 61. Mukherjee R, Davies PJ, Crombie DL, Bischoff ED, Cesario RM, Jow L, Hamann LG, Boehm MF, Mondon CE, Nadzan AM, Paterniti Jr JR, Heyman RA 1997 Sensitization of diabetic and obese mice to insulin by retinoid X receptor agonists. *Nature* 386:407–410
 62. Hill JO, Peters JC 1998 Environmental contributions to the obesity epidemic. *Science* 280:1371–1374
 63. Barker DJ, Bull AR, Osmond C, Simmonds SJ 1990 Fetal and placental size and risk of hypertension in adult life. *Br Med J* 301:259–262
 64. Phillips DI, Hirst S, Clark PM, Hales CN, Osmond C 1994 Fetal growth and insulin secretion in adult life. *Diabetologia* 37:592–596
 65. Martyn CN, Barker DJ, Jespersen S, Greenwald S, Osmond C, Berry C 1995 Growth in utero, adult blood pressure, and arterial compliance. *Br Heart J* 73:116–121
 66. Yajnik C 2000 Interactions of perturbations in intrauterine growth and growth during childhood on the risk of adult-onset disease. *Proc Nutr Soc* 59:257–265
 67. Barker DJ, Martyn CN, Osmond C, Hales CN, Fall CH 1993 Growth in utero and serum cholesterol concentrations in adult life. *Br Med J* 307:1524–1527
 68. Lucas A 1998 Programming by early nutrition: an experimental approach. *J Nutr* 128:401S–406S
 69. Armitage JA, Khan IY, Taylor PD, Nathanielsz PW, Poston L 2004 Developmental programming of metabolic syndrome by maternal nutritional imbalance; how strong is the evidence from experimental models in mammals? *J Physiol* 561:355–377
 70. Masuno H, Kidani T, Sekiya K, Sakayama K, Shiosaka T, Yamamoto H, Honda K 2002 Bisphenol A in combination with insulin can accelerate the conversion of 3T3-L1 fibroblasts to adipocytes. *J Lipid Res* 43:676–684
 71. Masuno H, Okamoto S, Iwanami J, Honda K, Shiosaka T, Kidani T, Sakayama K, Yamamoto H 2003 Effect of 4-nonylphenol on cell proliferation and adipocyte formation in cultures of fully differentiated 3T3-L1 cells. *Toxicol Sci* 75:314–320
 72. Toschke AM, Koletzko B, Slikker Jr W, Hermann M, von Kries R 2002 Childhood obesity is associated with maternal smoking in pregnancy. *Eur J Pediatr* 161:445–448
 73. von Kries R, Toschke AM, Koletzko B, Slikker Jr W 2002 Maternal smoking during pregnancy and childhood obesity. *Am J Epidemiol* 156:954–961
 74. Oken E, Huh SY, Taveras EM, Rich-Edwards JW, Gillman MW 2005 Associations of maternal prenatal smoking with child adiposity and blood pressure. *Obes Res* 13:2021–2028
 75. Power C, Jefferis BJ 2002 Fetal environment and subsequent obesity: a study of maternal smoking. *Int J Epidemiol* 31:413–419
 76. Hill SY, Shen S, Locke Wellman J, Rickin E, Lowers L 2005 Offspring from families at high risk for alcohol dependence: increased body mass index in association with prenatal exposure to cigarettes but not alcohol. *Psychiatry Res* 135:203–216
 77. Umesono K, Murakami KK, Thompson CC, Evans RM 1991 Direct repeats as selective response elements for the thyroid hormone, retinoic acid, and vitamin D3 receptors. *Cell* 65:1255–1266
 78. Perlmann T, Rangarajan PN, Umesono K, Evans RM 1993 Determinants for selective RAR and TR recognition of direct repeat HREs. *Genes Dev* 7:1411–1422
 79. Blumberg B, Mangelsdorf DJ, Dyck JA, Bittner DA, Evans RM, De Robertis EM 1992 Multiple retinoid-responsive receptors in a single cell: families of retinoid "X" receptors and retinoic acid receptors in the *Xenopus* egg. *Proc Natl Acad Sci USA* 89:2321–2325
 80. Blumberg B, Bolado J Jr., Derguini F, Craig AG, Moreno TA, Chakravarti D, Heyman RA, Buck J, Evans RM 1996 Novel retinoic acid receptor ligands in *Xenopus* embryos. *Proc Natl Acad Sci USA* 93:4873–4878
 81. Blumberg B, Sabbagh Jr W, Juguillon H, Bolado Jr J, van Meter CM, Ong ES, Evans RM 1998 SXR, a novel steroid and xenobiotic-sensing nuclear receptor. *Genes Dev* 12:3195–3205
 82. Tabb MM, Sun A, Zhou C, Grun F, Errandi J, Romero K, Pham H, Inoue S, Mallick S, Lin M, Forman BM, Blumberg B 2003 Vitamin K2 regulation of bone homeostasis is mediated by the steroid and xenobiotic receptor SXR. *J Biol Chem* 278:43919–43927
 83. Grun F, Blumberg B 2003 Identification of novel nuclear hormone receptor ligands by activity-guided purification. *Methods Enzymol* 364:3–24
 84. Grun F, Venkatesan RN, Tabb MM, Zhou C, Cao J, Hemmati D, Blumberg B 2002 Benzoate X receptors α

- and β are pharmacologically distinct and do not function as xenobiotic receptors. *J Biol Chem* 277:43691–43697
85. Livak KJ, Schmittgen TD 2001 Analysis of relative gene expression data using real-time quantitative PCR and the $2^{-\Delta\Delta C(T)}$ method. *Methods* 25:402–408
86. Bourguet W, Ruff M, Chambon P, Gronemeyer H, Moras D 1995 Crystal structure of the ligand-binding domain of the human nuclear receptor RXR- α . *Nature* 375:377–382
87. Allegretto EA, McClurg MR, Lazarchik SB, Clemm DL, Kerner SA, Elgort MG, Boehm MF, White SK, Pike JW, Heyman RA 1993 Transactivation properties of retinoic acid and retinoid X receptors in mammalian cells and yeast. Correlation with hormone binding and effects of metabolism. *J Biol Chem* 268:26625–26633
88. Lehmann JM, Moore LB, Smith-Oliver TA, Wilkison WO, Willson TM, Kliewer SA 1995 An antidiabetic thiazolidinedione is a high affinity ligand for peroxisome proliferator-activated receptor γ (PPAR γ). *J Biol Chem* 270:12953–12956
89. Nieuwkoop P, Faber J 1994 Normal table of *Xenopus laevis* (Daudin). 2nd ed. New York: Garland Publishing, Inc.
90. Rugh R 1962 Experimental embryology: techniques and procedures. 3rd ed. Minneapolis: Burgess Publishing Co.



Molecular Endocrinology is published monthly by The Endocrine Society (<http://www.endo-society.org>), the foremost professional society serving the endocrine community.

Original Paper

PTOVI: a novel testosterone-induced atherogenic gene in human aorta

Y Nakamura,¹ T Suzuki,¹ K Igarashi,⁴ J Kanno,⁴ T Furukawa,² C Tazawa,¹ F Fujishima,¹ I Miura,¹ T Ando,⁴ N Moriyama,¹ T Moriya,¹ H Saito,⁵ S Yamada³ and H Sasano^{1*}

¹Department of Pathology, Tohoku University School of Medicine, Sendai, Japan

²Department of Molecular Pathology, Tohoku University School of Medicine, Sendai, Japan

³Department of Radiology, Tohoku University School of Medicine, Sendai, Japan

⁴Division of Toxicology, the Biological Safety Research Centre, National Institute of Health Sciences, Tokyo, Japan

⁵Department of Radiology, Sendai Medical Centre, Sendai, Japan

*Correspondence to:

Dr H Sasano, Department of Pathology, Tohoku University School of Medicine, 2-1

Seiryō-machi, Aoba-ku, Sendai, 980-8575 Japan.

E-mail: hsasano@patholo2.med.tohoku.ac.jp

Abstract

There are gender differences in the development of atherosclerosis, possibly owing to differences in sex steroid hormone action and/or metabolism. One of the atherogenic effects of testosterone is thought to be androgen receptor (AR)-mediated vascular smooth muscle cell (VSMC) proliferation. However, the detailed mechanism of this effect, particularly the identity of the genes associated with VSMC proliferation, remains largely unknown. Therefore, we first employed microarray analysis and, subsequently, quantitative RT-PCR to analyse RNA expression in AR-positive human VSMCs treated with testosterone in order to detect testosterone-induced genes associated with cell proliferation. We further examined whether the genes identified were involved in cell proliferation using small interfering RNA (siRNA) transfection. Expression of the gene products was then evaluated in human aorta with various degrees of atherosclerosis in order to evaluate the clinical relevance of the findings. Both microarray and quantitative RT-PCR analyses demonstrated marked induction of the human prostate overexpressed protein 1 (*PTOVI*) gene by testosterone in the cell lines: this gene was recently identified as a novel androgen-induced gene involved in prostate tumour cell proliferation. Inhibition of *PTOVI* by transfection of its corresponding siRNA suppressed testosterone-induced cell proliferation. In human aorta, *PTOVI* immunoreactivity in the nuclei of neointimal VSMCs was abundantly detected in male aorta with mild atherosclerotic changes compared with female aorta or male aorta with severe atherosclerotic changes. These findings indicate that the *PTOVI* gene is androgen-responsive in VSMCs and that it may play an important role in androgen-related atherogenesis in the human aorta, particularly early atherosclerosis in the male aorta, through regulating proliferation of neointimal VSMCs.

Copyright © 2006 Pathological Society of Great Britain and Ireland. Published by John Wiley & Sons, Ltd.

Keywords: vascular smooth muscle cells; androgen receptor; testosterone; cell proliferation; *PTOVI*

Received: 25 October 2005

Revised: 8 February 2006

Accepted: 4 March 2006

Introduction

There is an important, well-documented, gender difference in coronary heart disease risks, with earlier onset of disease and excess mortality in male subjects [1–3]. Athero-protective effects of oestrogens on vascular structure and function have been proposed as one of the most important mechanisms accounting for this gender difference [4]. On the other hand, an association between androgens and atherosclerosis continues to be disputed. Androgens have been considered to reduce the incidence of ischaemic myocardial disease in men, but they have also been reported to exert atherogenic effects on the human cardiovascular system through promoting plaque formation and enhancing monocyte adhesion to endothelial cells [5–8]. It

has been demonstrated that testosterone exerts direct atherogenic effects by promoting cell proliferation through an initial interaction with the androgen receptor (AR) in vascular smooth muscle cells (VSMCs) *in vitro* [9]. However, unlike oestrogens, the possible effects of testosterone on atherogenesis and/or anti-atherogenesis have not been extensively studied. It is therefore important to study the detailed mechanisms of these direct effects of testosterone on the human cardiovascular system.

In this study, we first screened for testosterone-induced genes involved in the proliferation of VSMCs using microarray analysis in cell lines derived from AR-positive human VSMCs. We then confirmed the results by employing other *in vitro* studies. As testosterone induced marked overexpression of *PTOVI* in

these assays, we subsequently examined the levels of expression of PTOVI protein in VSMCs in samples of the human abdominal aorta obtained at autopsy.

Materials and methods

Vascular smooth muscle cells

Two types of human dedifferentiated VSMCs, ie HUVS-112D (derived from human umbilical cord), and T/G HA-VSMC (derived from human aorta) were commercially obtained from American Type Culture Collection (Manassas, VA, USA) [10,11]. We examined whether these cells expressed AR using an RT/real-time PCR with a light Cycler System using DNA binding dye SYBR Green I, and immunoblotting with AR polyclonal antibody (Santa Cruz Biotechnology, Inc, Santa Cruz, CA, USA), as reported previously [10,12].

GeneChip microarray assay

The VSMCs above were cultured until a sub-confluent state was achieved. The medium was then replaced with fetal bovine serum (FBS)-free and phenol red-free medium to arrest cell proliferation. After 24 h, the medium was replaced again with phenol red-free and FBS-free medium in the presence of testosterone (10 nM) or vehicle (0.1% ethanol). After incubation for 2 h, the cells were subsequently subjected to total RNA extraction for microarray analysis. Isolated total RNA was labelled as described in the Affymetrix (Santa Clara, CA, USA) GeneChip Expression Analysis Technical Manual (revision 3), as previously described [10]. The ratios represent the values up- or down-regulated by 10 nM testosterone treatment compared with control. We independently repeated the same experiment twice. Genes for which the average ratios increased more than 1.5-fold in both experiments using 10 nM testosterone treatment were considered up-regulated via AR when compared with control values [13]. When studying the potential functions of these genes, we used the homepage of the HUGO Gene Nomenclature Committee (<http://www.gene.ucl.ac.uk/nomenclature>, accessed 28 March 2006) for further examination of whether any had been previously reported to be involved in cell proliferation and to be associated with androgen effects. In this study, among the genes that were found to be significantly induced by testosterone treatment by microarray analysis, we regarded a gene that was up-regulated, and was known to be associated with both cell proliferation and androgenic effects, as a target gene.

Quantitative real-time PCR

After achieving sub-confluence and following growth arrest states of the VSMCs as described above,

the medium was replaced again with phenol red-free and FBS-free F12-K medium with testosterone (10 nM), testosterone (10 nM) with flutamide, an AR-blocker (100 nM), or vehicle. After incubation for 2 h, the cells were subsequently subjected to total RNA extraction for RT/real-time PCR analysis, described previously [10]. mRNA levels for the target gene *PTOVI* were determined in each VSMC as a ratio relative to glyceraldehyde-3-phosphate dehydrogenase (*GAPDH*), and evaluated as a ratio (%) compared with that of each control cDNA. The analyses with real-time PCR were repeated three times. Table 1 summarizes the primers used [14].

siRNA preparation, transfection, and cell count assay

Small interfering RNAs (siRNAs) corresponding to *PTOVI* (Table 2) were synthesized based on results of a previous report, and were transfected into the VSMCs [15]. These VSMCs were seeded in a 24-well plate at an initial concentration of 50 000 cells/well with F-12K medium containing 2% FBS and were cultured until a sub-confluent status was achieved. The medium was then replaced with phenol red-free and FBS-free medium to arrest cell proliferation. After 24 h, transfection experiments of siRNA for endogenous gene targeting (10 nM or 100 nM) were carried out using RNAiFect™ transfection reagent (Qiagen, Valencia, CA, USA). After transfection, the cells were incubated in phenol red-free medium containing 2% dextran-coated, charcoal-stripped FBS with testosterone (10 nM) or vehicle (0.1% ethanol) for 24 h. We measured the number of cells in each sample as described above with Cell Counting Kit-8 system (Wako, Tokyo, Japan) after incubation for 48 h. We also examined the number of cells treated with

Table 1. Primer sequences used in RT-PCR analysis

cDNA	Sequence	Size (bp)
AR	Forward 5'-CTCACCAAGCTCCTGGACTC-3'	246
	Reverse 5'-CAGGCAGAAGACATCTGAAG-3'	
GAPDH	Forward 5'-TGAACGGGAAGCTCACTGG-3'	307
	Reverse 5'-TCCACCACCCTGTTGCTGTA-3'	
PTOVI	Forward 5'-CACCATCCCTCCATGTTGCTG-3'	250
	Reverse 5'-TCTTCATTGGCCTCATCCCC-3'	

Table 2. Sequences used in siRNA transfection analysis

cDNA	Sequence
PTOVI	Sense r(CAACAAGUUUCUGGCAUGG)dTdT
	Antisense r(CCAUGCCAGAAACUUGUUG)dTdT
Negative control	Sense r(UUCUCCGAACGUGUCACGU)dTdT
	Antisense r(ACGUGACACGUUCGGAGAA)dTdT

The target gene in this study (*PTOVI*) was determined by microarray analysis. The sequences of *PTOVI* siRNAs are based on a previous report [15].

transfection of negative control siRNA with scrambled sequences (Table 2), and treated with testosterone (10 nM) or vehicle. In order to evaluate transfection efficiency, we examined relative *PTOVI* mRNAs levels in these cells at 24 h after transfection of the specific siRNAs. The mRNA levels in each VSMC were calculated as a ratio relative to *GAPDH*, and were normalized to the ratio after transfection of negative control siRNA (10 nM).

Quantitative RT-PCR analysis of *PTOVI* mRNA expression in human aorta

Samples of human abdominal aorta were collected at autopsy from patients without a history of hormone replacement therapy. Autopsies were performed on 32 subjects (16 male, 16 female; mean 60.7 ± 3.3 years) in Tohoku University Hospital (Sendai, Japan) within 2 h post mortem. The Ethics Committee at Tohoku University School of Medicine approved the research protocol for this study. Aortic specimens were tentatively classified into the following four groups according to the sex of the deceased patient and degree of atherosclerosis, as previously described: group A = male, mild atherosclerosis, corresponding to groups I–III in the American Heart Association (AHA) classification; group B = male, advanced atherosclerosis, corresponding to groups IV–VI in the AHA classification; group C = female, mild atherosclerosis; and group D = female, advanced atherosclerosis [10,11]. The distribution of the cases among these groups was as follows: A, 8 cases (mean 44.3 ± 10.6 years); B, 8 cases (mean 71.3 ± 3.7 years); C, 8 cases (mean 52.0 ± 3.9 years); and D, 8 cases (mean 75.0 ± 2.1 years), respectively. For RT/real-time PCR analysis, these specimens were treated according to our previous report [10]. The mRNA levels for *PTOVI* and *AR* in each sample are given as a ratio relative to *GAPDH*, and evaluated as a ratio (%) compared with that of each control cDNA.

Immunohistochemical analysis for *PTOVI* protein expression in human aorta

Details of immunohistochemical procedures have been previously described [10,11]. We used immunostaining with diaminobenzidine (DAB) for immunohistochemical analysis of *PTOVI* protein (using a monoclonal anti-human *PTOVI* antibody; Novocastra Laboratories, Newcastle, UK) and *AR* (using a monoclonal antibody for human *AR*; Dako Corporation, Carpinteria, CA, USA). We also used double immunostaining with DAB and Vector Blue as colorimetric reagents, with a combination of monoclonal antibodies for α -smooth muscle actin (α -SMA; Dako Corporation), for macrophages (PG-M1, Dako Corporation), and for leukocytes (human leukocyte common antigen antibody (LCA; Dako Corporation) in adjacent tissue sections. After determining the areas for evaluation by simultaneous observation using a multi-headed light microscope, three authors (YN, TS, and HS)

independently evaluated immunoreactivity. Scoring of immunoreactivity was performed based on our previous reports with some modifications [10,16]. When *PTOVI* protein was immunolocalized to the cytoplasm, the relative immunoreactivity in each specimen was classified into the following three groups: 2 = more than 50% positive cells; 1 = more than 10% and less than 50% positive cells; and 0 = negative or less than 10% positive cells, respectively [16]. When *PTOVI* protein immunoreactivity was detected in the nuclei, the relative immunoreactivity in each specimen was evaluated by the percentage of immunoreactivity, ie the labelling index (LI) [10]. When inter-observer differences were $>5\%$, the three aforementioned authors re-evaluated these discrepant immunostained slides simultaneously using a multi-headed light microscope, and the mean value was obtained.

Statistical analysis

Values for all results were given as the mean \pm standard error of the mean (SEM). Results of quantitative RT-PCR, cell count assay, and the relative immunoreactivity for protein in the nuclei were analysed using one-way analysis of variance followed by unpaired *t*-test for comparisons between two groups. Results of immunohistochemistry of cytoplasmic protein were analysed using the χ^2 -test. Statistical differences between immunoreactivity for *PTOVI* protein and *AR* were evaluated using Spearman's rank correlation. A *p* value <0.05 was considered significant in this study.

Results

Characterization of two VSMC cell lines

By RT-PCR analysis, both HUVS-112D cells and T/G HA-VSMC cells expressed *AR* mRNA (Figure 1A). In addition, *AR* protein was demonstrated in both of these cell lines by immunoblotting analysis (110 kD) (Figure 1B). Relative levels of *AR* mRNA and protein expression in these cells were approximately 5–10% of those in LNCaP cells that were examined in parallel (data not shown).

Gene chip microarray assay

Table 3 summarizes 11 genes that were up-regulated by testosterone treatment in both types of VSMC in duplicated microarray analysis. Among these genes, human prostate tumour overexpressed protein 1, ie *PTOVI* was detected in both of these VSMCs. Recently, *PTOVI* has been reported to be induced by androgen and to be involved in cell cycle regulation [14,15,17]. *AGTR2* was also reported to be associated with androgenic effects, but it is unknown whether *AGTR2* is involved in cell growth [18]. Therefore we focused our subsequent studies on *PTOVI* as

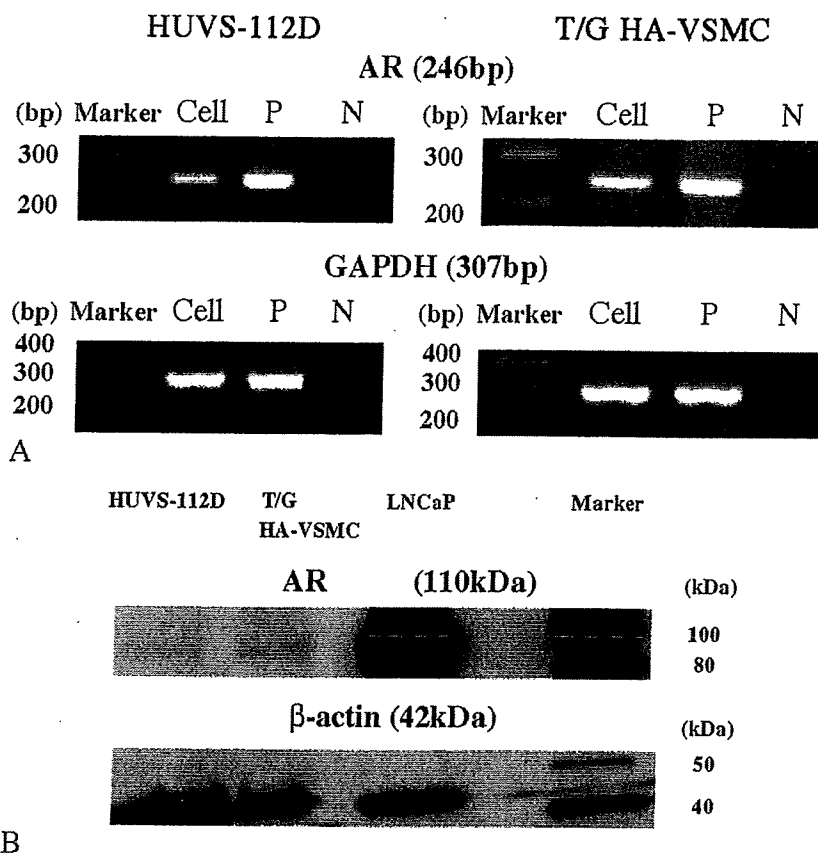


Figure 1. (A) Results of RT/real-time PCR analysis for AR and GAPDH in two cultured human VSMCs (HUVS-112D, and T/G HA-VSMC), positive controls, and negative controls. Cell = each type of cultured vascular smooth muscle cell; P = positive control (LNCaP prostate cancer cell line); N = negative control (no cDNA), respectively). (B) Immunoblotting analysis of AR and β -actin in HUVS-112D, T/G HA-VSMC, and LNCaP cells. Total protein was extracted, and 60 μ g protein from each cell was loaded. Immunoblotting analysis demonstrated both AR (110 kD) and β -actin protein (42 kD) in all cells

Table 3. Ratios of gene expression determined by GeneChip microarray analysis after testosterone treatment of cultured VSMCs for 2 h

Gene symbol	HUVS-112D	T/G HA-VSMC	Function	Association with androgen (reference)
PAK7	3.9	3.6	Neurite development	Unknown
PIK3R4	1.7	3.3	Cell signalling	Unknown
CELSR1	1.9	3.1	Cell adhesion	Unknown
CACNA1G	2.5	2.9	Calcium channel	Unknown
AGTR2	2.2	2.5	Regulator of aldosterone secretion	Koike <i>et al</i> [18]
INVS	2.7	3.6	Renal tubular development	Unknown
GPR77	3.5	2.6	Cell signalling	Unknown
CASP10	3.3	2.8	Apoptosis	Unknown
AP4S1	2.1	2.5	Formation of cell structure	Unknown
TIA-2	1.7	2.7	Membrane glycoprotein	Unknown
PTOVI	1.8	2.0	Cell growth/mitogenesis	Benedit <i>et al</i> [14]

'Ratios' represent the mean ratios of expression levels of each gene mRNA in duplicate experiments compared with control.

an androgen-responsive gene possibly involved in the proliferation of human VSMCs.

PTOVI mRNA expression in VSMCs after androgen treatment

Testosterone significantly increased *PTOVI* mRNA levels in AR-positive VSMCs compared with controls in both of these cell lines ($p < 0.05$) (Figure 2). However, testosterone with flutamide, an AR-blocker

(100 nM), did not increase its mRNA expression in either of these cells ($p < 0.05$) (Figure 2).

PTOVI siRNA transfection and cell proliferation assay

Quantitative RT-PCR analysis demonstrated that *PTOVI* mRNA levels were decreased in a dose-dependent manner in the cells transfected with *PTOVI* siRNAs (Figure 3A). After transfection of negative

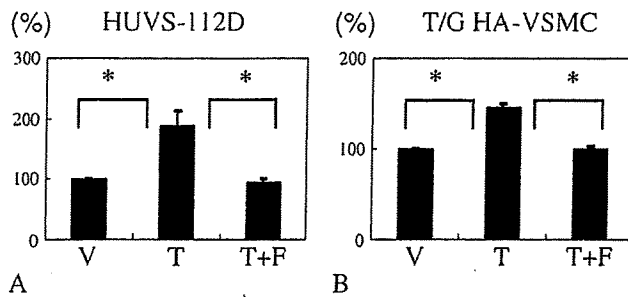


Figure 2. Results of RT/real-time PCR analysis for *PTOVI* in HUVS-112D (A) and T/G HA-VSMC cells (B) among cells treated with vehicle (V) (control), testosterone (T) alone (10 nM), and T (10 nM) with flutamide (F), an AR-blocker (100 nM), respectively after 2 h ($*p < 0.05$)

control siRNA (10 nM), testosterone promoted cell proliferation significantly in both of these cell lines

($p < 0.05$) (Figure 3B). However, testosterone with transfection of *PTOVI* siRNA (10 nM and 100 nM) did not increase cell proliferation in these two cell lines (Figure 3B).

PTOVI mRNA expression in human aorta

The results of RT/real-time PCR analysis demonstrated the presence of specific single bands for AR and *PTOVI* in human aorta (Figure 4A). The relative abundance of *PTOVI* mRNA was significantly greater in male aorta with a mild degree of atherosclerotic changes (group A) than in those of other groups (groups B, C, and D) ($p < 0.05$) (Figure 4B). The relative abundance of AR mRNA was also significantly greater in male aorta with a mild degree of atherosclerotic change (group A) than in male aorta with a severe

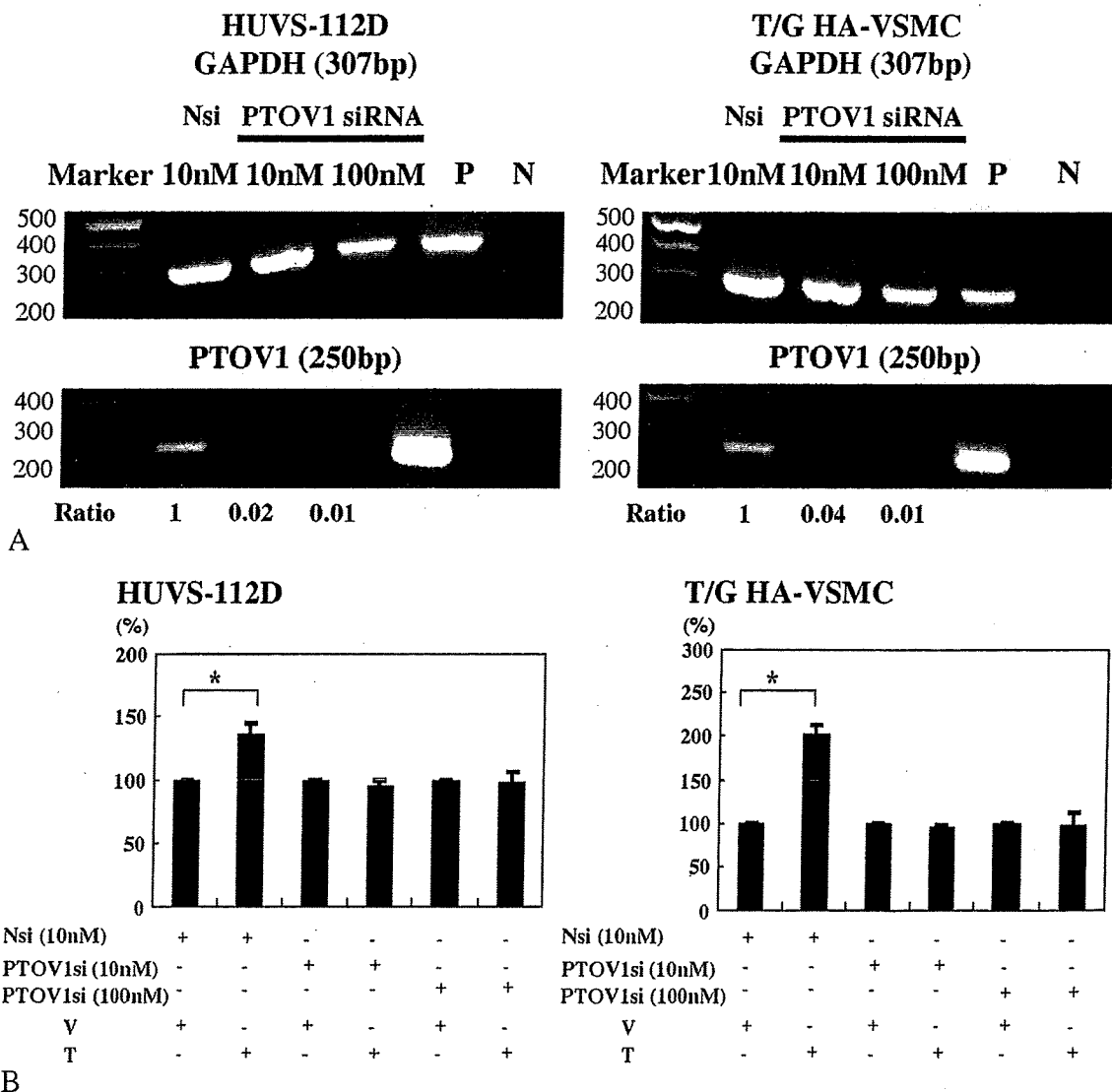


Figure 3. (A) Expression of *PTOVI* and *GAPDH* mRNAs at 24 h after transfection of *PTOVI* siRNA (10 nM or 100 nM) or negative control siRNA (Nsi) (10 nM) in HUVS-112D and T/G HA-VSMC cells detected by real-time PCR, respectively. *GAPDH* mRNA expression was monitored as an internal control. The ratio of *PTOVI*/*GAPDH* was calculated and values were normalized to the ratio obtained from the negative control transfection of Nsi (10 nM). P = positive controls (LNCaP prostate cancer cell lines); N = negative controls (no cDNAs), respectively. (B) The relative levels of cell numbers in HUVS-112D and T/G HA-VSMC cells among cells treated with vehicle (V) (0.1% ethanol) and testosterone (T) alone (10 nM) after transfection of *PTOVI* siRNA (*PTOVI*si) (10 nM or 100 nM) or negative control siRNA (Nsi) (10 nM) ($*p < 0.05$)

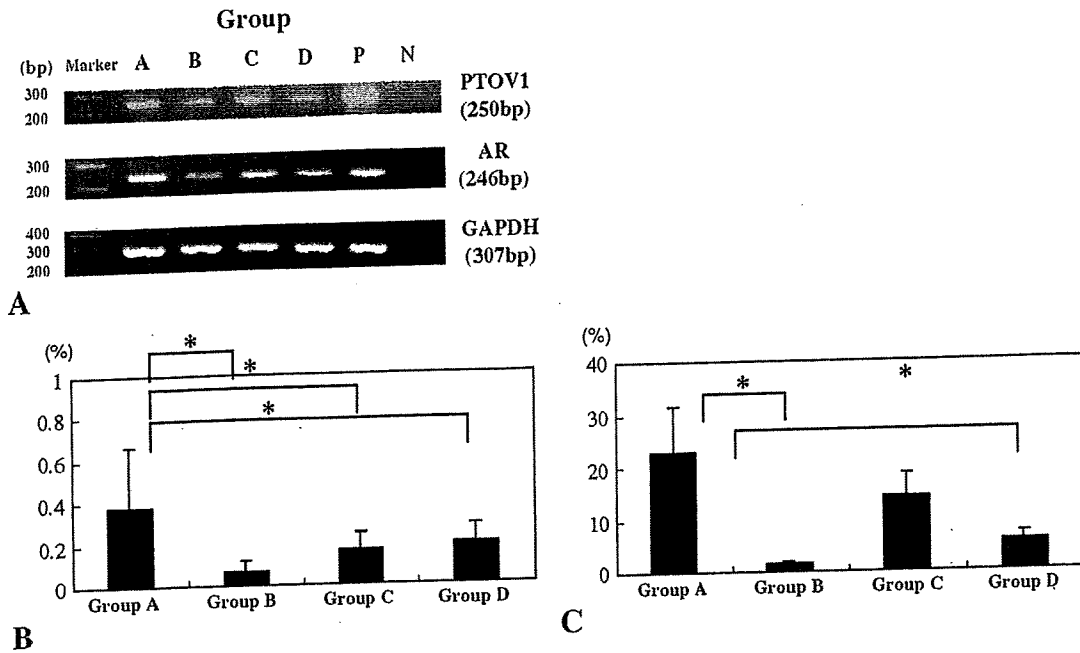


Figure 4. (A) Results of RT/real-time PCR analysis for *PTOVI* in human aortas. Bands for PCR products were detected as specific single bands (246 bp for AR, 250 bp for *PTOVI*, and 307bp for GAPDH). The amplified products were run on a 2% agarose gel stained with ethidium bromide. Representative photographs for these RT/real-time PCR gene products are illustrated. A = aorta from a 38-year-old man with mild atherosclerotic change; B = aorta from a 72-year-old man with severe atherosclerotic change; C = aorta from a 45-year-old woman with mild atherosclerotic change; D = aorta from a 76-year-old post-menopausal woman with severe atherosclerotic change; P = positive controls; N = negative controls. (B) Results for *PTOVI* mRNA expression levels ($*p < 0.05$). (C) Results for AR mRNA expression levels ($*p < 0.05$).

degree of atherosclerosis (group B) and in female aorta with a severe degree of atherosclerosis (group D) ($p < 0.05$) (Figure 4C).

Immunohistochemistry for *PTOVI* in human aorta

PTOVI protein was expressed in both the nucleus and the cytoplasm of VSMCs in each group examined (Figures 5 and 6). AR protein was expressed in the nuclei of VSMCs in each group (Figures 5 and 6). However, none of the LCA- or PG-M1-positive cells demonstrated any *PTOVI* immunoreactivity (Figure 5). The relative levels of *PTOVI* immunoreactivity in the nuclei of neointimal VSMCs were significantly higher in male aorta with a mild degree of atherosclerotic change (group A) than in those of the other groups examined (groups B, C, and D) (Figure 6A). In addition, AR-positive cells in the neointima were also significantly more abundant in male aorta with a mild degree of atherosclerotic changes (group A) than in those of the other groups (groups B, C, and D) ($p < 0.05$) (Figure 6E). There was also a significant positive correlation between AR and *PTOVI* immunoreactivity in the nuclei of VSMCs in the neointima ($p < 0.05$) (data not shown). AR-positive cells in the tunica media were significantly more abundant in male aorta with a mild degree of atherosclerotic change (group A) than in male aorta with a severe degree of atherosclerosis (group B) and in female aorta with a mild degree of atherosclerosis (group C) ($p < 0.05$) (Figure 6F). However, there

were no significant differences in *PTOVI* immunoreactivity in the cytoplasm of cells in the neointima or in the nucleus and/or cytoplasm of cells in the tunica media among these groups (Figure 6B, C, and D).

Discussion

In our present study, results of both microarray and quantitative RT-PCR analyses all indicated that *PTOVI* is one of the genes induced by testosterone via AR-dependent pathways in cultured human VSMCs. In addition, siRNA analysis demonstrated that *PTOVI* is involved in AR-mediated VSMC proliferation. Results of both quantitative RT-PCR and immunohistochemical studies in human aorta obtained at autopsy further demonstrated that *PTOVI*, as well as AR, detected in the nuclei of neointimal VSMCs was abundant in relatively young male aorta at an early stage of atherosclerosis.

PTOVI has been known to be involved in stimulation of cell proliferation [14,15,17]. This gene is a mitogenic factor that shuttles between nucleus and cytoplasm in a cell cycle-dependent manner in prostate carcinoma cells [14,15,17]. In addition, *PTOVI* overexpression induced cell proliferation and facilitated entry of prostate carcinoma cells into the S phase [14,15,17]. Therefore, these findings all indicated that *PTOVI* may play a very important role in the proliferation of VSMCs. However, it is also true that other atherogenic effects on human VSMCs, such as promotion of PDGF-induced VSMC proliferation,

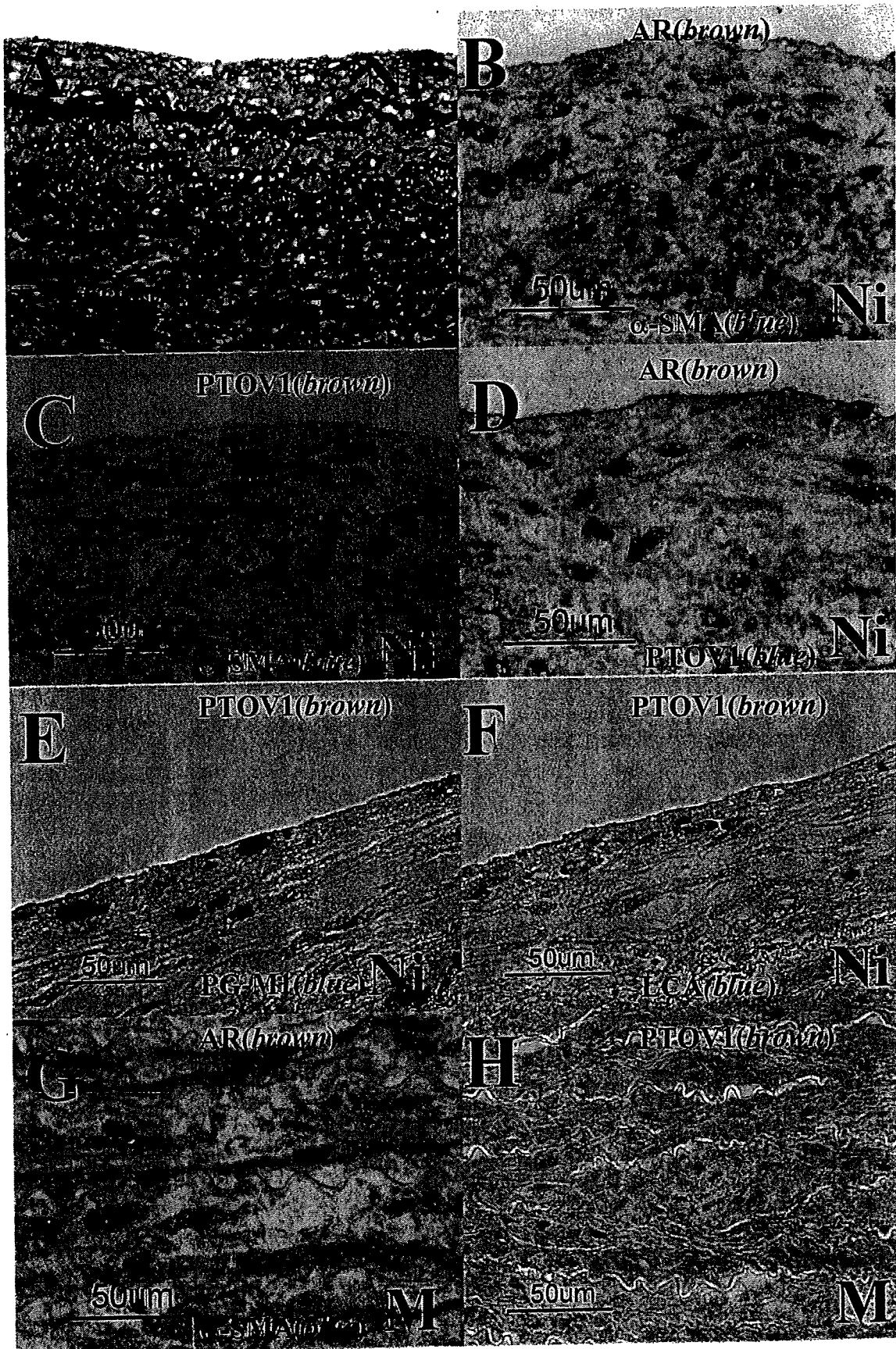


Figure 5. Modified Masson Goldner's stains (A), double-immunohistochemical staining for AR and α -muscle actin (α -SMA) (B), for PTOVI and α -SMA (C), for AR and PTOVI (D), for PTOVI and PG-MI (E), for PTOVI and leukocyte common antigen (LCA) (F) in the neointima, double-immunohistochemical staining for AR and α -SMA (G) and immunohistochemical staining for PTOVI (H) in the media of an abdominal aorta specimen obtained from a 38-year-old man with a mild degree of atherosclerosis (group A). Immunopositive cells appear brown as a result of DAB colorimetric reaction and blue as a result of Vector Blue colorimetric reaction. Double-immunopositive cells are confirmed. Ni = neointima; M = media